lubricants

MDPI

Review

Research Progress on Tribological Properties of High-Entropy Alloys

Shuai Zhang [1], Zhaofeng Wang [2,*], Wenqing Lin [1] and Haoyu Guo [1]

[1] School of Automotive and Mechanical Engineering, Liaoning Institute of Science and Engineering, Jinzhou 121013, China; zhangshuai24@126.com
[2] Faculty of Electrical and Control Engineering, Liaoning Technical University, Huludao 125105, China
* Correspondence: wangzhaofeng0412@126.com; Tel./Fax: +86-04295310894

Abstract

As a new type of alloy system composed of five or more principal components, high-entropy alloys demonstrate outstanding comprehensive performance in the field of friction and wear through the synergistic effects of the high-entropy effect, lattice distortion effect, hysteresis diffusion effect and cocktail effect. This paper systematically reviews the research progress on the friction and wear properties of high-entropy alloys. The mechanisms of metal elements such as Al, Ti, Cu and Nb through solid solution strengthening, second-phase precipitation and oxide film formation were analyzed emphatically. And non-metallic elements such as C, Si, and B form and strengthen the regulation laws of their tribological properties. The influence of working conditions, such as high temperature, ocean, and hydrogen peroxide on the friction and wear behavior of high-entropy alloys by altering the wear mechanism, was discussed. The influence of test conditions such as load, sliding velocity and friction pair matching on its friction coefficient and wear rate was expounded. It is pointed out that high-entropy alloys have significant application potential in key friction components, providing reference and guidance for the further development and application of high-entropy alloys.

Keywords: high-entropy alloys; friction and wear; working conditions; wear mechanism

check for updates

Received: 6 July 2025
Revised: 24 July 2025
Accepted: 30 July 2025
Published: 1 August 2025

Citation: Zhang, S.; Wang, Z.; Lin, W.; Guo, H. Research Progress on Tribological Properties of High-Entropy Alloys. *Lubricants* **2025**, *13*, 342. https://doi.org/10.3390/lubricants13080342

Copyright: © 2025 by the authors. Licensee MDPI, Basel, Switzerland. This article is an open access article distributed under the terms and conditions of the Creative Commons Attribution (CC BY) license (https://creativecommons.org/licenses/by/4.0/).

1. Introduction

Under the background of the continuous pursuit of performance breakthroughs in the field of materials science, high-entropy alloys, as a new type of alloy system that subverted the traditional design concept, are becoming a frontier hotspot in the research of metallic materials with their unique multi-principal component structure and excellent comprehensive performance [1,2]. By virtue of the high-entropy effect, lattice distortion effect, hysteresis diffusion effect and cocktail effect, high-entropy alloys not only demonstrate multiple properties such as high hardness, high heat resistance, strong corrosion resistance, excellent wear resistance and oxidation resistance, but also break the inherent limitations of traditional alloys in performance balance [3,4].

In the field of mechanical engineering, wear is the primary form of material failure. Approximately 80% of moving parts fail due to wear, which not only causes huge material and energy losses but also may lead to serious safety hazards [5]. The development of high-performance anti-wear and lubricating materials has always been a key issue that materials science urgently needs to overcome. Although traditional alloys have optimized their strength, hardness and toughness through alloying, heat treatment, deformation

processing and other means, under extreme working conditions such as high temperature, high pressure, strong corrosion and high-speed friction environment, their anti-wear and lubrication performance are difficult to meet the strict requirements of modern industry for reliability and durability.

The emergence of high-entropy alloys provides a new path to break through this predicament. Its unconventional chemical structure and multiple synergistic effects make it show significant advantages in the field of friction materials. On the one hand, through the coordination of composition regulation and preparation process, the precise design of the microstructure can be achieved, thereby optimizing the tribological properties. On the other hand, its unique microstructure characteristics enable it to maintain stable anti-wear performance in special functional requirements such as corrosion resistance, radiation resistance, low temperature, and catalysis, effectively filling the application gap of traditional alloys [6–8].

Based on this, this paper systematically reviews the research progress on the friction and wear properties of high-entropy alloys. Firstly, this article explains the definition and scope of high-entropy alloys and the synergistic mechanism of the four core effects. Furthermore, from the perspective of alloying element regulation, the influence laws of metal elements such as Al, Ti, and Cu through solid solution strengthening, second-phase precipitation, and oxide film formation, as well as non-metal elements such as C, Si, and B through strengthening phase formation on friction and wear performance are deeply analyzed. Combining extreme working conditions such as high temperature, ocean, and hydrogen peroxide, this paper explores its regulatory effect on tribological behavior by altering the wear mechanism. At the same time, the paper elaborates on the significant influences of test conditions such as load, sliding velocity, and friction pair matching on the coefficient of friction and wear rate. Finally, the application potential of high-entropy alloys in key friction components in fields such as aerospace, marine engineering, and mechanical manufacturing is explored, providing theoretical references and technical support for the wear-resistant design and engineering application of high-entropy alloys.

2. Concept of High-Entropy Alloys

2.1. Definition of High-Entropy Alloys

The initial definition of high-entropy alloys was based on the mixed entropy value of the alloys. In statistical thermodynamics, entropy is a thermodynamic property related to the degree of system chaos and is a measure of the degree of system chaos. Mixed entropy is the change in the entropy value of the system caused by the different configurations of atoms of different principal elements being mixed with each other [9]. The mixed entropy reaches its maximum value when there is no concentration gradient in the alloy system, which is known as the system reaching equilibrium. It is generally believed that if the influence of other configurations on the entropy value of the alloy system is not considered, the atomic arrangement configuration has the greatest impact on the entropy value of the multi-principal high-entropy alloy system. Therefore, the mixed entropy caused by atomic arrangement is the main contributor to the entropy value change of high-entropy alloy systems [10].

The entropy value S of the system can be calculated by the Boltzmann equation, as shown in Equation (1).

$$S = k\ln W \tag{1}$$

where k represents the Boltzmann constant, and W indicates the total number of possible microscopic states in the system.

In a regular solid solution type alloy system, the expression of the mixing entropy ΔS_{mix} of n principal element alloy systems can be as follows

$$\Delta S_{mix} = -R\sum x_i \ln x_i \quad (2)$$

where R is the molar gas constant, and x_i is the molar ratio of the i principal element in the alloy system. According to Boltzmann's assumption on entropy and chaos, when the ratio of each principal element atom in the alloy system is equal in moles, the mixed entropy of this n principal element alloy system reaches its maximum value, which can be specifically expressed as

$$\Delta S_{mix} = R\ln n \quad (3)$$

From the above formula, it can be seen that as the number of principal components in the alloy system increases, its mixing entropy keeps growing. When two principal components are mixed in equal molar ratios to form an alloy, the mixing entropy of the alloy system is 0.69R. When the five principal components are mixed in equal molar ratios to form an alloy, the mixing entropy of the alloy system is 1.61R. When the number of alloy components is greater than 13, the change of mixing entropy tends to level off. Initially, based on the above-mentioned theory of mixed entropy, researchers classified alloys into low-entropy alloys, medium-entropy alloys, and high-entropy alloys according to the magnitude of mixed entropy [11,12]. When the mixing entropy of the alloy system is lower than 0.69R, it is a low-entropy alloy. At this time, the corresponding alloy system is a solid solution alloy with two principal components in equal molar ratios. When the mixing entropy of the alloy system is higher than 1.61R, it is a high-entropy alloy. At this time, the corresponding alloy system is a solid solution alloy with five principal components in equal molar ratios. When the mixed entropy of the alloy system is between 0.69R and 1.61R, it is a medium-entropy alloy, and the number of principal elements is between two and four principal elements. However, the above definition is only applicable to regular solid solution alloy systems and can only serve as a rough classification range in practical situations [13].

Professor Yeh believes that ΔS_{mix} = 1.5R is a necessary condition for resisting the strong interatomic bonding force at high temperatures, and the relatively low mixing entropy of the alloy system is difficult to compete with the bonding energy. Therefore, based on the magnitude of the mixed entropy that the alloy system possesses when it is in a random solid solution state, the alloy world can be classified into the following three categories [14,15].

(1) Low-entropy alloys: alloys mainly composed of one or two components, such as traditional alloys, ΔS_{mix} is less than R.
(2) Medium-entropy alloys: alloys mainly binary to quaternary, the mixing entropy is between R and 1.5R.
(3) High-entropy alloys: alloys mainly consisting of five to thirteen elements, when the mixing entropy ΔS_{mix} is greater than 1.5R.

This composition design of high-entropy alloys, which breaks away from the traditional "1 to 2 main elements as the base", places them in the central area of the phase diagram, offering nearly unlimited space for composition regulation and possibilities for organizational structure [16]. The comparison between high-entropy alloys and traditional alloys is shown in Table 1.

In recent years, with the continuous advancement of research on high-entropy alloys, their definition scope has gradually expanded. When defining high-entropy alloys, researchers no longer limit their evaluation criteria to the mixed entropy value of the alloy system, but incorporate more alloys with excellent comprehensive performance into the category of high-entropy alloys [17–23].

Table 1. Performance comparison between traditional alloys and high-entropy alloys.

Dimension	Traditional Alloys	High-Entropy Alloys
Composition design	Based on 1–2 elements (proportion > 50%)	5 or more principal elements (atomic ratio 5–35%)
Phase diagram position	Biased towards endpoints (dominated by a single principal element)	Located in the central region (mixed by multiple principal elements)
Microstructure	Prone to form intermetallic compounds or brittle phases	Tend to form simple solid solutions (FCC/BCC, etc.)
Performance characteristics	Single performance is prominent, but it is difficult to coordinate multiple performances	Balanced comprehensive performance, breaking through traditional performance bottlenecks

2.2. Characteristics of High-Entropy Alloys

As a new type of material, the unique properties of high-entropy alloys can be attributed to four core effects: the high-entropy effect, the lattice distortion effect, the hysteresis diffusion effect and the cocktail effect [24]. These effects are mutually synergistic, interrelated and have a synergistic effect, profoundly influencing the microstructure and performance of the alloy, and endowing high-entropy alloys with excellent comprehensive properties distinct from traditional alloys.

In traditional alloys, due to the scarcity of main elements, the probability of forming intermetallic compounds or brittle phases is relatively high. The presence of these phases often reduces the toughness and overall performance of the alloy. In high-entropy alloys, when five or more main elements are uniformly mixed, the high-entropy effect acts like a "structural stabilizer", which makes the alloy system tend to form simple solid solution structures with lower free energy, such as face-centered cubic FCC, body-centered cubic BCC, and closely arranged hexagonal HCP. This is because in a high-entropy state, the energy barriers that need to be overcome to form complex intermetallic compounds increase significantly, and alloys are more likely to exist in the form of uniform solid solutions [25,26]. The high-entropy effect has been confirmed from many aspects [27–31]. The schematic diagram of the high-entropy effect promoting the formation of solid solutions is shown in Figure 1. Here, ΔG_{mix} represents the change in Gibbs free energy, and ΔS_{mix} represents the change in the mixed entropy.

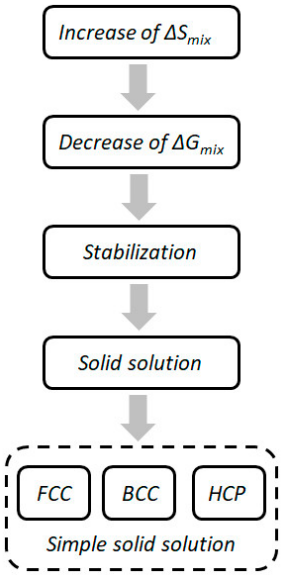


Figure 1. Schematic diagram of the promotion of solid solution formation by high-entropy effect.

The atomic radius, electronegativity and valence electron concentrations of each principal element in high-entropy alloys are different, and these differences are the root causes of the lattice distortion effect [32,33]. As shown in Figure 2, each atom may be surrounded by different types of atoms, and the originally regularly arranged lattice structure is disrupted, thereby causing lattice distortion. Lattice distortion makes the stress field inside the lattice uneven, and this uneven stress field greatly increases the resistance to dislocation movement. Dislocations, as common defects in crystals, and their mobility directly affect the plastic deformation and strength of materials. In high-entropy alloys with severe lattice distortion, dislocations are difficult to slip, thereby significantly enhancing the strength and hardness of the alloy [34]. In addition, lattice distortion also affects the diffusion path of atoms and has a significant impact on the subsequent phase transformation and precipitation behavior of the alloy [35].

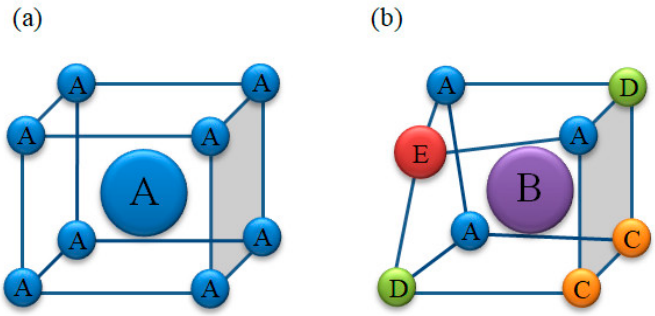


Figure 2. Schematic diagram of the lattice distortion effect: (**a**) BBC no lattice distortion; (**b**) BBC severe lattice distortion.

The hysteresis diffusion effect of high-entropy alloys stems from the significant inhibition of atomic migration by their unique multi-principal component chemical composition and complex crystal structure. In high-entropy alloys, the differences in atomic radii among various metal elements lead to severe lattice distortion, forming a physical barrier that hinders atomic migration [36–38]. Atomic diffusion needs to overcome a higher potential energy barrier, and its diffusion activation energy is significantly higher than that of pure metals [39–42]. Meanwhile, short-range ordered structures or complex electron clouds formed among multiple principal elements overlap, creating "energy traps" in the lattice. When atoms diffuse, they need to break the constraints of various chemical bonds, further increasing the difficulty of diffusion. Furthermore, when multiple elements in an alloy diffuse simultaneously, a competitive effect occurs due to their different diffusion rates, similar to the "traffic congestion" where atoms interfere with each other in the lattice, resulting in a significant reduction in the overall diffusion efficiency. This hysteresis diffusion effect enables high-entropy alloys to effectively inhibit grain growth and the precipitation of the second phase in high-temperature environments, thereby enhancing the thermal stability of the material. During the process of corrosion and wear, it slows down the medium penetration and material loss and enhances the corrosion resistance and wear resistance [43,44].

The cocktail effect of high-entropy alloys was first proposed by Ranganthan's team [45]. The cocktail effect stems from the performance advantages generated by the synergy of multiple main elements. By analogy with cocktails, a unique flavor is formed by fusing multiple components [46,47]. This effect refers to the fact that high-entropy alloys break through the traditional alloy composition design model based on a single or dual main element by uniformly mixing five or more main elements in a specific proportion, achieving the collaborative optimization of multiple properties, as shown in Figure 3. In high-entropy alloy systems, the different main elements each possess unique performance attributes,

such as enhancing strength, improving corrosion resistance, and improving oxidation resistance. When these elements coexist, they are not simply superimposed in terms of performance, but rather, through complex physical and chemical interactions, they produce mutually reinforcing or complementary synergistic effects. This effect enables high-entropy alloys to break through the trade-off limitations of traditional alloys in terms of strength and toughness, wear resistance and corrosion resistance, etc., and obtain comprehensive properties such as high strength, high toughness, excellent corrosion resistance, and good thermal stability simultaneously [48–50].

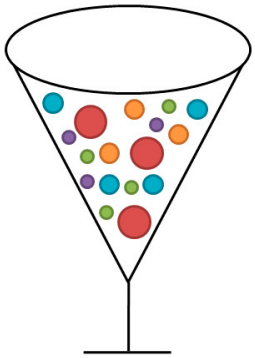


Figure 3. Schematic diagram of cocktail effect.

The above four major effects of high-entropy alloys are interdependent and synergistic, jointly shaping their excellent comprehensive performance. Figure 4 describes the lattice structure that leads to the four major effects of high-entropy alloys [51]. The high-entropy effect, as the cornerstone of structural stability, promotes the formation of a uniform solid solution in the alloy, laying the foundation for the exertion of other effects. The lattice distortion effect significantly enhances the strength and hardness of the alloy by disrupting the lattice structure. The hysteresis diffusion effect significantly reduces the atomic diffusion rate through complex interactions among multiple components, effectively enhancing the high-temperature stability, corrosion resistance and wear resistance of the alloy. The cocktail effect breaks through the linear superposition limitation of traditional alloy properties through the synergistic complementarity of multiple alloying elements, achieving an optimized balance of various properties such as strength, toughness, and oxidation resistance.

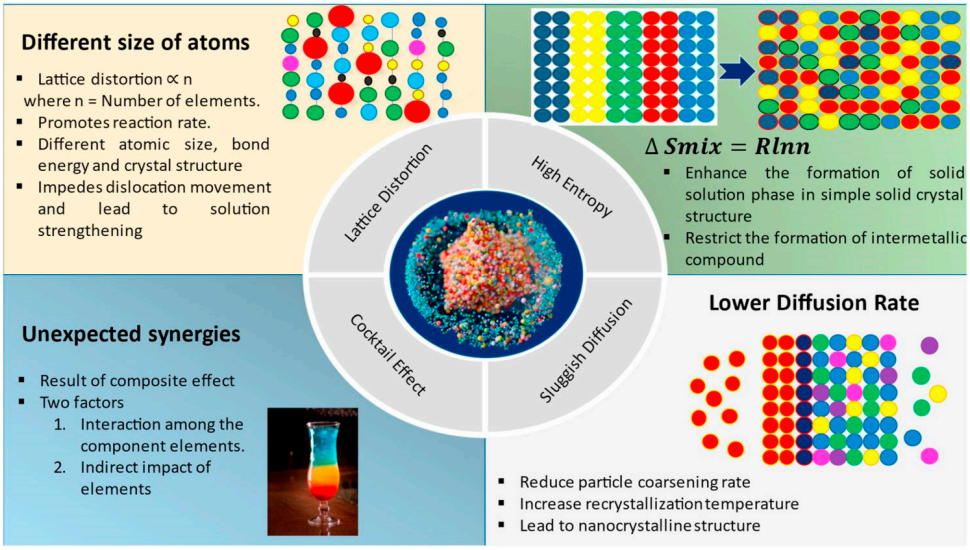


Figure 4. Lattice arrangement that leads to different core effects [51].

The four major effects are deeply intertwined from multiple dimensions such as thermodynamics, crystal structure, kinetics and composition synergy. They not only subvert the performance boundaries of traditional alloys but also open up a brand-new path for the innovative application of materials under extreme working conditions.

3. Influence of Alloying Elements on the Tribological Properties of High-Entropy Alloys

This section mainly summarizes the influence of alloying elements on the friction and wear properties of high-entropy alloys. The common metallic and non-metallic elements in the high-entropy alloy system are shown in Table 2.

Table 2. Common metallic and non-metallic elements in high-entropy alloy systems.

Common Element	Examples for Element Classification
Light metal elements	Al, Li, Be, Mg, Ca
Transition metal elements	Ti, Cu, Mn, Fe, Co
Refractory metal elements	Nb, Mo, W, Hf
Non-metallic elements	C, Si, B, N

The addition of each element in the above table will have a certain impact on the performance of high-entropy alloys. Now, the elements that can have a significant impact on the friction and wear performance of high-entropy alloys are analyzed in sequence.

3.1. Metal Elements

3.1.1. Light Metal Elements

The Al element can stabilize the BCC phase, cause lattice distortion, refine grains, and thereby enhance the wear resistance of high-entropy alloys. Wu et al. [52] found that in $Al_xCoCrCuFeNi$, an increase in Al content could promote the transformation of the alloy from a face-centered cubic structure to a body-centered cubic structure, thereby enhancing the alloy's hardness and reducing its wear rate. Li et al. [53] found that in the $CrFeNiAl_xSi$ alloy, when x = 0.6, the wear resistance of the alloy was the best. Al forms a solid solution for strengthening and simultaneously generates a dense oxide film, enhancing the wear resistance of the alloy. Cheng et al. [54] investigated the influence of Al content on the friction and wear properties of $FeCoCrNiMnAl_x$ high-entropy alloy over a wide temperature range, revealing the mechanisms of solid solution strengthening and oxide film formation. As shown in Figure 5, the study found that with an increase in Al content, the friction coefficient of the $FeCoCrNiMnAl_x$ alloy decreased from 0.45 to 0.32. Figure 6 compares the three-dimensional morphology of the worn surfaces of each alloy at room temperature and 800 °C. As can be seen from the figure, the wear surface of the Al1 alloy at 800 °C only has shallow grooves and a small amount of plastic deformation, while the surface of the Al0 alloy has deep tear pits and material accumulation. The three-dimensional morphology visually presents a significant decrease in the wear rate.

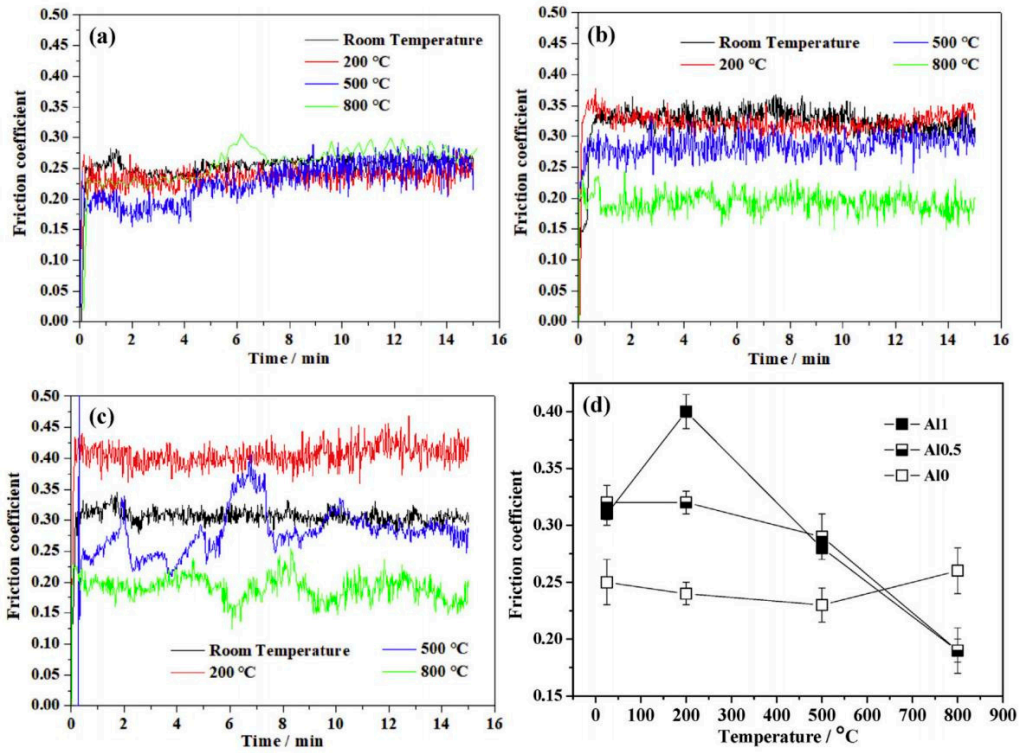


Figure 5. Friction coefficient curves of (**a**) Al0, (**b**) Al0.5, (**c**) Al1 alloys, (**d**) average friction coefficient [54].

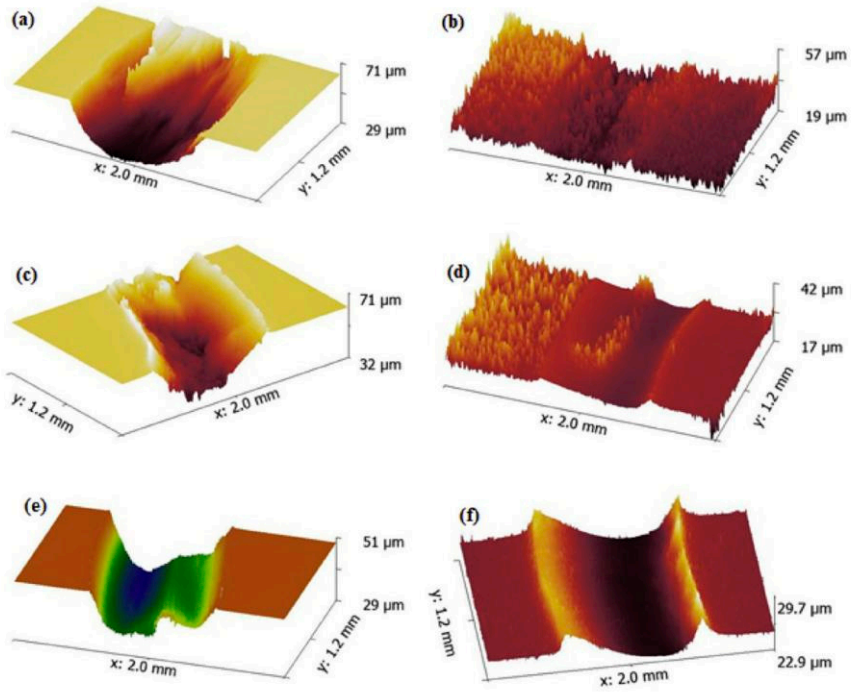


Figure 6. Three-dimensional morphologies of the worn surfaces of (**a**,**b**) Al0, (**c**,**d**) Al0.5 and (**e**,**f**) Al1 alloys: (**a**,**c**,**e**) room temperature and (**b**,**d**,**f**) 800 °C [54].

3.1.2. Transition Metal Elements

The addition of the Ti element has also been confirmed to enhance the hardness and wear resistance of high-entropy alloys. Wang et al. [55] added Ti to the CoCrFeMnNi high-entropy alloy coating and found that the room-temperature wear mechanism of the CoCrFeMnNi high-entropy alloy coating was abrasive wear, while the wear mechanism

of the $(CoCrFeMnNi)_{85}Ti_{15}$ high-entropy alloy coating at room temperature was mainly oxidation wear and contact fatigue. The formed $(CoCrFeMnNi)_{85}Ti_{15}$ coating, due to the addition of Ti, promotes the precipitation of the second phase, and has a high-temperature wear resistance 5.5 times that of the CoCrFeMnNi high-entropy alloy coating. Ye et al. [56] investigated the influence of Ti content on the wear resistance of $CoCu_{0.5}FeNiVTi_x$ using a disc-type wear testing machine. The research found that the wear forms of the high-entropy alloys were adhesive wear and abrasive wear, and the precipitation of the second phase at x = 1 brought the wear resistance to the best state. Xu et al. [57] investigated the properties of AlCoCrFeNi alloy and Ti-containing alloy $AlCoCrFeNiTi_{0.5}$ during unidirectional and bidirectional sliding wear processes. The results show that the addition of Ti increases the hardness of the alloy and enhances the wear resistance of the high-entropy alloys.

Cu, as a relatively common transition metal element, can also affect the performance of high-entropy alloys to a certain extent. Mukanov et al. [58] studied the influence of the introduction of the Cu element on high-entropy alloys. As shown in Figure 7, Figure 7a presents the dynamic variation of the friction coefficient with the number of cycles of $CoCrCu_xFeNi$ alloys with different Cu contents during the friction test. Figure 7b compares the depth and width of the wear trajectories of alloys with different Cu contents. It can be seen that the results show that the wear grooves of $CoCrCu_{0.25}FeNi$ (5 at. % Cu) are the shallowest. Figure 7c presents the microscopic characteristics of the worn surface from a 3D perspective. The oxide layer on the surface of the sample with a low Cu content (≤5 at. %) is continuous, with only shallow grooves existing. Verma et al. [59] also investigated the influence of Cu on the wear resistance of CoCrFeNi and found that after adding Cu to CoCrFeNi, the wear rate of the obtained CoCrFeNiCu decreased at both room temperature and high temperature, and the hardness of the alloy increased.

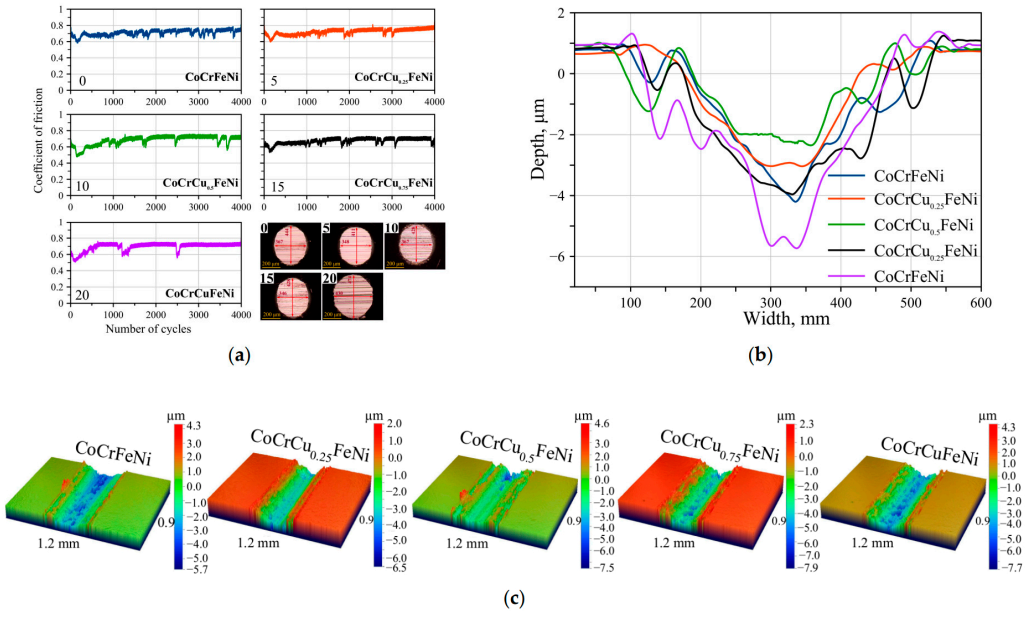


Figure 7. (**a**) Coefficient of friction as a function of the number of cycles; (**b**) wear trajectories of alloys with different Cu contents; (**c**) 3D images of the wear tracks [58].

The Fe element, as one of the commonly used elements in high-entropy alloys, has the function of stabilizing the FCC phase. Hsu et al. [60] studied the influence of the variation of Fe content in $AlCoCrFexMo_{0.5}Ni$ on the wear resistance. It was found that the microstructure of the alloy with Fe content increasing from x = 0.6 to x = 2.0 changed from "dendritic" to "polycrystalline", and the wear resistance decreased. High-entropy alloys with low iron content showed better wear resistance.

Shu et al. [61] investigated the use of Co instead of Fe to enhance the amorphous formation ability of laser cladding FeCoCrBNiSi high-entropy alloy coatings. They found that an increase in the iron–cobalt ratio would reduce the proportion of amorphous phases in the coating, intensify oxidative wear at high temperatures, and lower the high-temperature wear resistance of the alloy. Kumar et al. [62] investigated the frictional behavior of the $Al_{0.4}$FeCrNiCox high-entropy alloy (with x being 0, 0.25, 0.5, and 1.0, respectively). As shown in Figure 8, it is the optical microscopic image of the worn surface of the $Al_{0.4}FeCrNiCo_x$ (x = 0, 0.25, 0.5, 1.0 mol) high-entropy alloy under a sliding speed of 2 m/s, a sliding distance of 1000 m and a normal load of 10 N. Here, the influence of Co content on the morphology of the worn surface can be intuitively reflected. In Figure 8a, there is no Co addition. At this time, shallow scratches and micro-grooves parallel to the sliding direction can be seen on the worn surface. There is a small amount of plastic deformation of the material locally, but the overall wear marks are uniform, with no obvious oxide layer peeling or deep damage areas. In Figure 8b, when a small amount of Co is added, the scratch depth increases, local deep grooves appear, and material flow traces can be seen in some areas. The roughness of the worn surface is significantly higher than that in Figure 8a. When the Co content is further increased, as shown in Figure 8c, the worn surface presents irregular grooves and microcracks at this time. In some areas, material spalling pits appear, and the scratch directions are disordered, showing obvious fatigue wear characteristics. In Figure 8d, a large amount of Co addition leads to deep grooves, severe plastic deformation and large-scale spalling on the worn surface. Obvious material accumulation can be seen at the scratch edge, and the metal substrate is exposed in some local areas.

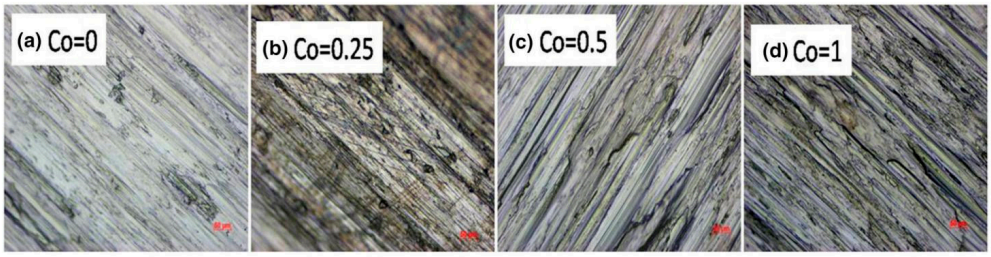


Figure 8. Micrographs of worn surfaces of $Al_{0.4}FeCrNiCo_x$ (**a**) Co = 0; (**b**) Co = 0.25; (**c**) Co = 0.25; (**d**) Co = 1 [62].

3.1.3. Refractory Metal Elements

Refractory metal elements are also important elements that affect the phase formation and microstructure of high-entropy alloys. Adding Nb element to high-entropy alloys can usually improve their wear resistance. Cheng et al. [63] prepared CoNiCuFeCr and CoNiCuFeCrNb coatings by plasma transfer arc melting and found that under the same wear test conditions, the addition of Nb could improve the wear resistance of the coatings by approximately 1.5 times. The research results of Yu et al. [64] indicated that Nb can enhance the hardness of $CoCrFeNiNb_x$ high-entropy alloy, making the wear at room temperature mainly abrasive wear. At a high temperature of 800 °C, due to the formation of a dense oxide layer, the wear rate is nearly zero. An increase in Nb content will intensify adhesive wear at 400 °C, and oxidative wear and mechanical wear above 600 °C will become the main mechanisms. Liu et al. [65] pointed out that in the $CoCrNiNb_x$ medium-entropy alloys, Nb promotes the formation of the BCC phase, refines the grains and increases the hardness. When x is within the appropriate range, the friction coefficient of the alloy decreases and the wear rate also drops, enhancing the wear resistance of the alloy. Figure 9 presents the SEM image of the worn surface of Nb_x. Among them, the a1–d1 image on the right is the enlarged image corresponding to the marked yellow square area in the

a–d image on the left. In Figure 9a, when x = 0, that is, when Nb is not added, there are deep furrows and a large amount of adhered wear debris on the alloy surface, forming a hilly accumulation. The wear mechanism is mainly characterized by severe adhesive wear and plastic deformation. At this time, the hardness of the alloy is low, and the FCC phase is prone to plastic flow. When x = 0.385, as shown in Figure 9c, the worn surface is smooth at this time, with only shallow grooves and a small amount of oxide layer. The layered eutectic structure suppresses local plastic deformation and debris accumulation by evenly sharing frictional stress. When x = 0.5, as shown in Figure 9d, cracks, spalling pits and coarse wear debris appear on the surface at this time, and the wear mechanism changes to fatigue wear and abrasive wear. Excessive brittleness of the laves phase leads to the propagation of microcracks on the wear surface, and the rupture of the oxide film intensifies the material loss.

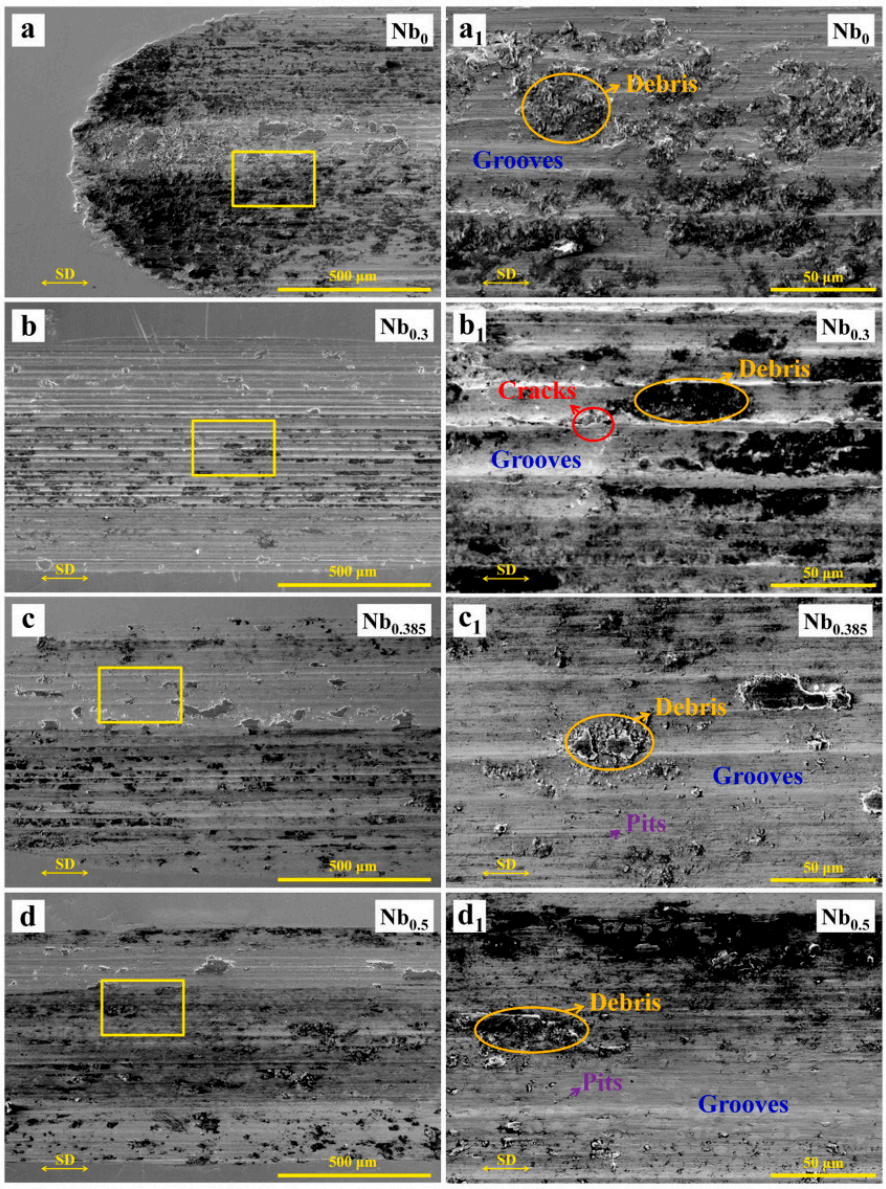


Figure 9. Micrographs of worn surfaces of $Al_{0.4}FeCrNiCo_x$ (**a**) Co = 0; (**b**) Co = 0.25; (**c**) Co = 0.25; (**d**) Co = 1; (**a_1**–**d_1**) enlarged image corresponding to the yellow square area in the left a-d image [65].

Adding a Mo element can effectively inhibit grain coarsening in the intermediate transition zone and has a significant effect on the cross-sectional microstructure after sliding wear. Deng et al. [66] increased the content of the Mo element in the $CoCrFeNiMo_x$

alloy under dry conditions at room temperature. The research finds that the addition of Mo increases the hardness of the alloy matrix, inhibits grain coarsening caused by surface frictional heat, and improves wear resistance. The research results of Chen et al. [67] show that the wear rate and friction coefficient of $CrFeNbTiMo_x$ refractory high-entropy alloy increase with the increase in Mo content, and the $CrFeNbTiMo_{1.0}$ sample doped with Mo exhibits the lowest wear rate and friction coefficient.

Some scholars have also conducted research on the influence of the addition of the W element on the wear resistance of alloys. The research results show that the addition of the W element can improve the room-temperature wear resistance of $CoCrFeNiW_x$ alloy. When conducting friction tests at 900 °C, the multi-component composite oxide friction glaze layer formed on the friction surface has a good anti-friction and anti-wear effect. In particular, the WO_3 produced by the oxidation of the W element significantly reduces the friction coefficient, thereby enhancing the high-temperature friction and wear performance of the alloy [68].

Table 3 presents a comparison of the influence of some metal elements on the tribological properties of high-entropy alloys.

Table 3. Comparison of the influence of metal elements on the tribological properties of high-entropy alloys.

Elements Added	Preparation Method	Material Composition	Experimental Parameter Conditions	Influence on Friction and Wear	References
Al	Laser sintering	$CrFeNiAl_xSi$	Load 20 N, abrasive grain 40 μm, time 5 min	Wear resistance is optimal when Al content reaches x = 0.6, in line with the positive correlation between hardness and wear resistance	[53]
Ti	Plasma cladding	$(CoCrFeMnNi)_{85}Ti_{15}$ coating	Load 25 N, room temperature 800 °C, rotating speed 300 rpm, time 20 min	Ti increases hardness by 6 times, and wear resistance is optimal at 400 °C	[55]
Cu	Arc melting	$CoCrFeNiCu_x$	Load 100 N, room temperature 600 °C, rotating speed 95 rpm, time 1000 s	Cu forms an oxide glaze layer, and high-temperature self-lubrication improves wear resistance	[59]
Fe	Arc melting	$AlCoCrFe_xMo_{0.5}Ni$	Load 29.4 N, speed 0.5 m/s, time 24 h	Increase in Fe reduces σ phase, wear resistance decreases, mainly abrasive wear	[60]
Co	Arc melting	$Al_{0.4}FeCrNiCo_x$	Load 5–20 N, sliding speed 0.5–2 m/s, room temperature	Increase in Co content reduces BCC phase and hardness, leading to decreased wear resistance	[62]
Nb	Arc melting	$CoCrFeNiNb_x$	Load 5 N, room temperature 800 °C, speed 0.188 m/s	A dense oxide layer forms at high temperatures, significantly reducing wear rate, at 800 °C, the oxide layer is glaze-like, and wear resistance is optimal	[64]
Mo	Spark plasma sintering + cold rolling	$CoCrFeNiMo_x$	Load 5 N/50 N, speed 6 mm/s	Mo solid solution strengthening improves hardness, inhibits grain coarsening, and reduces abrasive wear	[66]
W	Vacuum arc melting	$CoCrFeNiW_x$	Load 10 N, room temperature and 900 °C, speed 0.3 m/s	W addition increases high-temperature hardness, and high-temperature oxidation generates WO_3 to reduce friction coefficient	[68]

3.2. Non-Metallic Elements

In addition to metallic elements, some non-metallic elements will also be added to the ranks of improving the performance of high-entropy alloys. Xiao et al. [69] conducted a study on the situation of the C element in the $CoCrFeMnNiC_x$ alloy. Figure 10a visually presents the wear surface states of high-entropy alloys under different C contents. The wear trajectory of the CoCrFeMnNi alloy without C addition is the deepest. When x = 0.6, the wear trajectory of the $CoCrFeMnNiC_{0.6}$ alloy is the shallowest, with a uniform surface and no obvious accumulation of plastic deformation. It can be seen that the addition of the

C element can significantly reduce the degree of damage to the worn surface. Figure 10b visually reveals the correlation between C content and wear rate. As the C content increased from x = 0 to x = 0.6, the wear rate of the alloy decreased by an order of magnitude. When the C content continued to increase (x = 0.9, 1.2), the wear rate slightly rebounded but was still lower than that of the carbon-free alloy. This trend indicates that an appropriate proportion of C can enhance wear resistance, while the increase in porosity caused by excessive C will weaken this effect. Figure 10c summarizes the wear rate–hardness relationship between this system and other high-entropy alloys.

The Si element is also frequently used in the research of high-entropy alloys because it can form silicide strengthening phases or change the composition structure of the matrix. Jin et al. [70] studied the $AlCoCrFeNiSi_x$ high-entropy alloy and found that the addition of Si could enhance the hardness, compressive strength and wear resistance of the alloy, and the main wear mechanism was abrasive wear. Kumar et al. [71] found that an increase in Si content could improve the wear resistance of $CoCrCuFeNiSi_x$, mainly due to the solid solution strengthening effect caused by the atomic radius mismatch between Si and other elements. Xin et al. [72] also conducted a study on the doping of Si in high-entropy alloys, and the corresponding research results are shown in Figure 10. Figure 10a shows the changes in the friction coefficients of various materials at different temperatures. The friction coefficient of high-entropy alloys doped with Si is more stable, and it shows a downward trend with the increase in Si content and the rise in temperature. Figure 10b quantifies the differences in wear rates at different temperatures. With the increase in temperature, the wear of Stellite-6 first increases and then decreases. Among the Si-doped high-entropy alloys, the wear rate of Al02Si01 is the lowest at all temperatures. This intuitively demonstrates that an appropriate amount of Si (x = 0.1) can significantly enhance high-temperature wear resistance, while excessive Si (x = 0.5) will lead to an increase in the wear rate. In Figure 10c–f, the data of high-entropy alloys are circled with colored backgrounds to distinguish and compare their properties with those of Stellite-6 alloy.

Some scholars have also conducted relevant research on the addition of high-entropy alloys to element B. Liu et al. [73] studied the frictional properties of the $Al_{0.5}CoCrCuFeNiB_x$ high-entropy alloy. The research found that the addition of element B enhanced the hardness of the alloy, thereby improving its wear resistance accordingly. When the content of element B is relatively low ($x \leq 0.4$), the differences in frictional properties between alloy systems are relatively small. When the B content is relatively high ($x \geq 0.6$), the wear resistance of the alloy is significantly enhanced. Lin et al. [74] investigated the influence of the B content on the microstructure and properties of the FeCoCrNiAlB high-entropy alloy coating. The results show that with the increase in B content, the content of the BCC phase increases, the content of the eutectic structure decreases, and the wear resistance of the high-entropy alloy coating also increases. When the B content is 0.75, the wear resistance of the high-entropy alloy coating is the best.

This section systematically reviews the influence of laws and mechanisms of metallic and non-metallic elements on the friction and wear properties of high-entropy alloys. The research shows that among the metallic elements, Al significantly enhances the hardness and wear resistance of the alloys by stabilizing the BCC phase, causing lattice distortion and promoting the formation of dense oxide films, and there exists an optimal content range. Ti enhances high-temperature wear resistance by promoting the precipitation of the second phase. When Cu is added in appropriate amounts, it can form a continuous oxide layer to improve wear resistance. Excessive Fe content will reduce wear resistance due to microstructure transformation. Excessive addition of Co can easily lead to intensified fatigue wear. Nb optimizes wear resistance by refining grains and regulating phase structure. Mo can inhibit grain coarsening, but excessive amounts may deteriorate performance. W

exerts anti-friction effects by forming a WO_3 enamel layer at high temperatures. Among non-metallic elements, C reduces the wear rate by increasing hardness, but its content needs to be controlled to avoid an increase in porosity. Si enhances wear resistance through solid solution strengthening and the formation of silicides. B enhances wear resistance by increasing the content of the BCC phase and regulating the eutectic structure. Overall, various elements mainly regulate the friction and wear performance of high-entropy alloys by influencing phase composition, microstructure, mechanical properties and surface oxidation behavior. Moreover, most elements have an optimal addition range. Excessive or insufficient addition may lead to a decrease in wear resistance. This section provides an important reference for the composition design and tribological property optimization of high-entropy alloys.

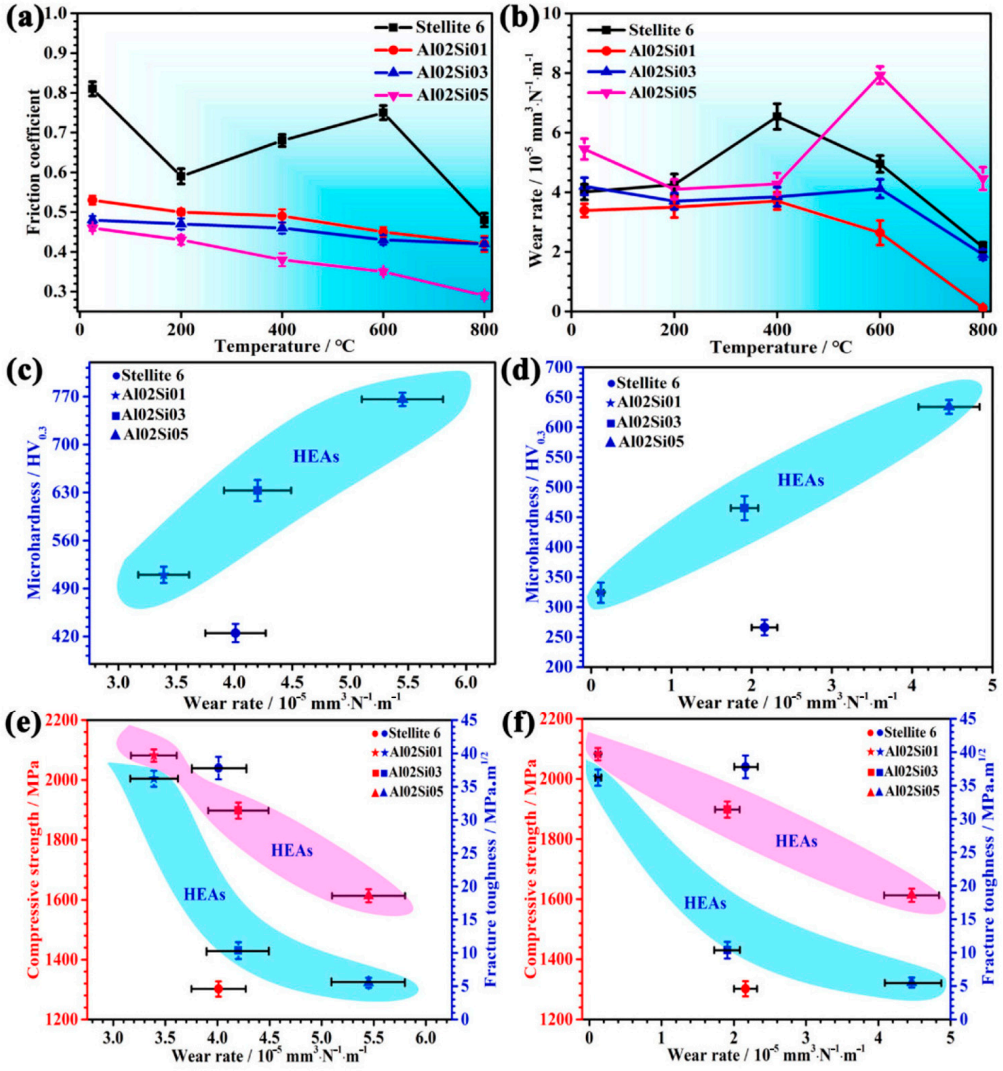


Figure 10. Comparison of tribological properties of different alloys from 25 °C to 800 °C: (**a**,**b**) the average friction coefficient and wear rate; (**c**–**f**) mechanical properties–wear rate relationship [72].

4. Influence of Friction Environment on Tribological Properties of High-Entropy Alloys

In practical engineering applications, the friction environment is one of the key factors determining the main wear mechanism of materials, which in turn affects the wear resistance of materials [75,76]. Analyzing the typical characteristics of high-entropy alloys under different friction environments, optimizing the alloying elements that promote the

occurrence of friction chemical reactions, and constructing high-entropy alloys that can meet the required performance under harsh working conditions by using the preferred alloying elements is conducive to the advantages and disadvantages of high-entropy alloys in engineering applications [77,78].

4.1. High-Temperature Environment

Liu et al. [79] investigated the wear resistance of $(CrMnFeHf)_{7.14}(TiTaV)_{23.81}$ high-entropy alloy at high temperatures. Figure 11 shows the 3D optical profile of the worn surface after the high-temperature dry sliding wear test, presenting the three-dimensional morphological characteristics of the wear trajectory of high-entropy alloys composites at different temperatures (room temperature, 200 °C, 400 °C, 600 °C). The figure visually presents the differences in depth and width of the wear trajectory at different temperatures through three-dimensional contours. It can be clearly observed from the figure that the shape of the wear trajectory changes significantly with the variation of temperature. At 200 °C, the wear trajectory is the deepest. As the temperature rises, the depth of the wear trajectory gradually decreases. At 600 °C, the wear trajectory is the shallowest, indicating that the material has the best wear resistance at this temperature. This is closely related to the effect of the oxide layer formed at high temperatures.

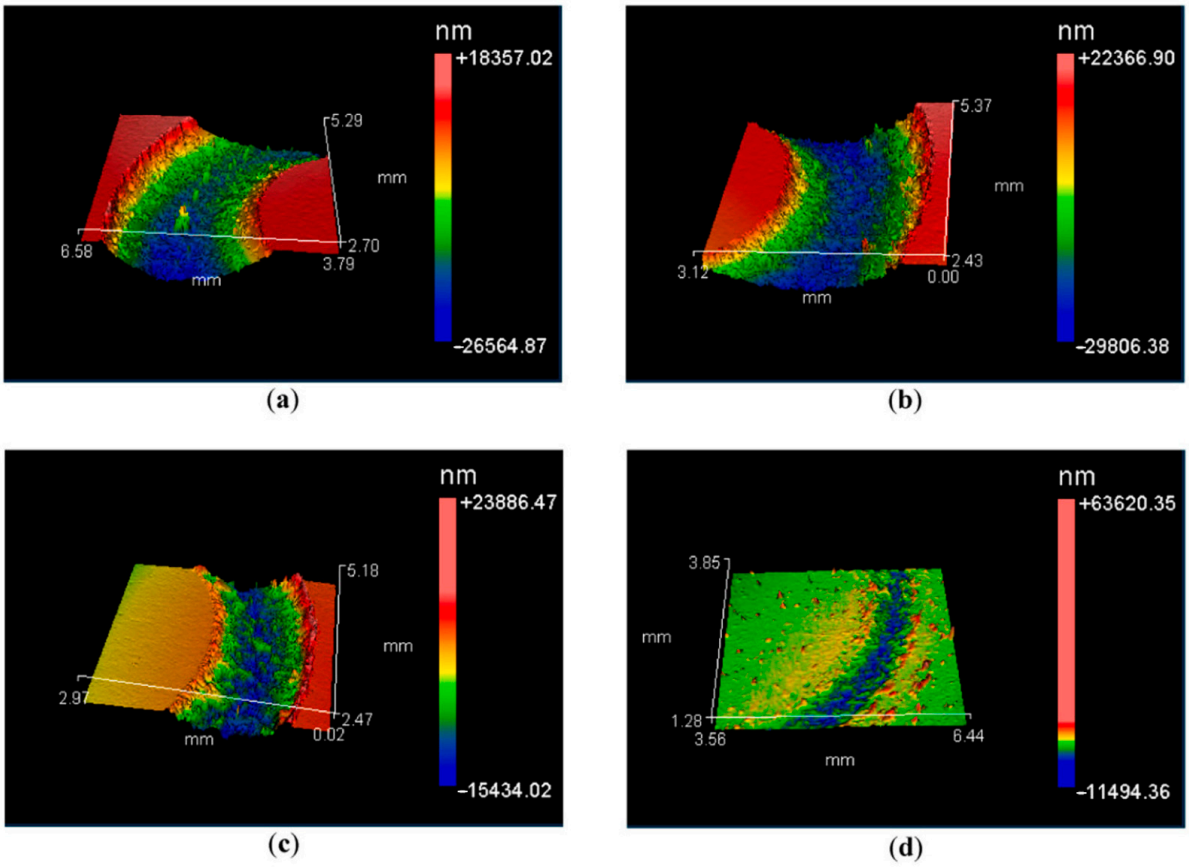


Figure 11. Surface profile of the worn surface at different temperatures: (**a**) room temperature; (**b**) 200 °C; (**c**) 400 °C; (**d**) 600 °C [79].

Jin et al. [80] investigated the high-temperature performance of laser cladding FeNi-CoAlCu high-entropy alloy coatings. Figure 12 reflects the influence of high temperature on the tribological properties of high-entropy alloys. The results show that the coefficient of friction is stable at 0.8–0.9 at room temperature, 200 °C and 400 °C. At 600 °C and 800 °C, the coefficient of friction significantly drops to around 0.3. This trend directly reflects the

regulation of alloy friction behavior by high-temperature environments, promoting the formation of oxide films and significantly reducing the coefficient of friction. In addition, Du et al. [81] also prepared an $Al_{0.25}$CoCrFeNi high-entropy alloy and conducted friction tests within the temperature range of 20 °C to 600 °C. The results show that due to high-temperature softening, the wear rate increases with the rise in temperature. However, due to the formation of the oxide film and the decrease in adhesion as the temperature rises, the coefficient of friction also decreases with the increase in temperature.

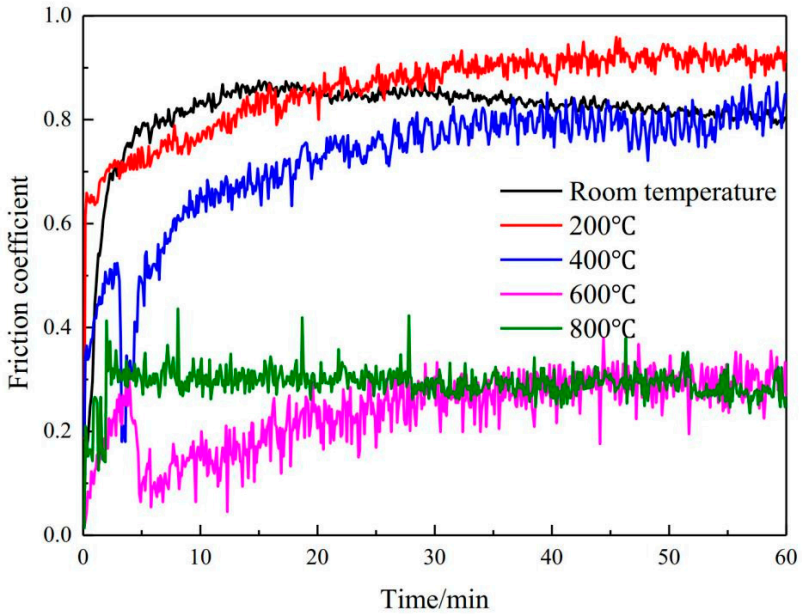


Figure 12. Friction coefficient at different temperatures [80].

4.2. Marine Environment

Most traditional alloys are prone to corrosion in seawater environments. Corrosion can deteriorate the worn surface and accelerate wear. Traditional corrosion-resistant alloys have relatively low hardness and strength, making it difficult to meet the requirements of wear resistance. Research has found that some metal elements, after corroding in seawater, can form self-lubricating oxides and hydroxides. Reference [82] describes the influence of the Marine environment on the high-entropy alloy coating of $AlCrFeNiW_{0.2}Ti_{0.5}$. The tribological properties of this coating are superior to those of Q235 steel and SUS304 stainless steel. The friction and wear of this coating are the least in seawater. This is because Ca^{2+}, Mg^{2+} and other substances in seawater form a protective friction film containing $CaCO_3$ and $Mg(OH)_2$, thereby isolating and reducing wear and friction, resulting in a decrease in the coefficient of friction and wear rate. Figure 13 shows the wear mechanism of the $AlCrFe_2Ni_2W_{0.2}Mo_{0.75}$ high-entropy alloy coating in seawater [83]. It clearly demonstrates the regulatory mechanism of the chemical changes and wear processes occurring on the surface of high-entropy alloys in the Marine environment. Seawater ions react with alloys to form products such as $Mg(OH)_2$ and $CaCO_3$, creating a friction film. Through isolation contact, lubrication and corrosion resistance, friction and wear are reduced. At the same time, alloying elements form metal oxides and hydroxides, and these products jointly form a friction film on the worn surface. This membrane isolation coating is in direct contact with the paired balls, providing lubrication and preventing Cl^- erosion, thereby reducing the coefficient of friction and wear rate.

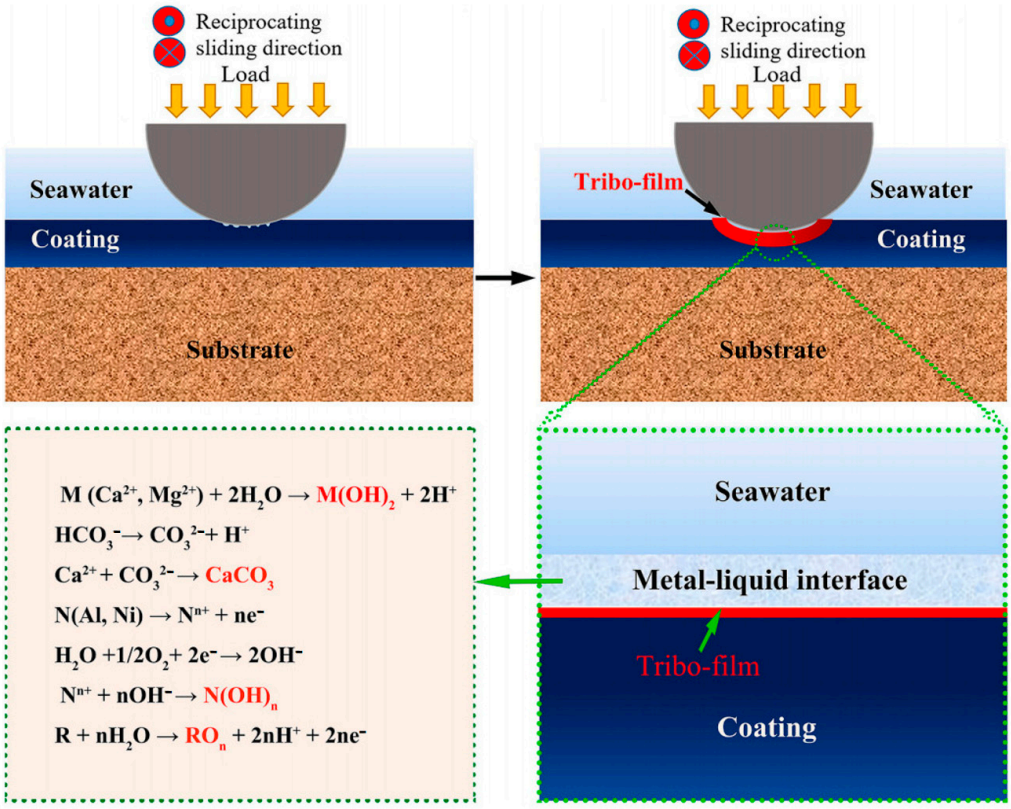


Figure 13. Schematic diagram of the wear mechanism in seawater [83].

4.3. H_2O_2 Environment

High-concentration hydrogen peroxide, as a green accelerator in the aerospace field, has compatibility issues with most metals due to its strong oxidizing and easily decomposable properties. It not only leads to severe oxidation and wear of compatible metals but may also cause serious friction and seizing under low-load and low-speed conditions. High-entropy alloys, with their unique performance advantages, have shown application potential in aerospace fields such as rocket engines containing hydrogen peroxide solutions, and are expected to solve the compatibility and wear problems between metals and hydrogen peroxide. Yu et al. [84] investigated the influence of hydrogen peroxide concentration on the tribological properties of the $AlCoCrFeNiTi_{0.5}$ high-entropy alloy. As the concentration of H_2O_2 increases, the friction and wear of the alloy improve, and there are no obvious wear marks on the surface. This is because a lubricating colloid film was formed, effectively inhibiting mechanical wear. Reference [85] investigated the friction properties of the $AlCoCrFeNiTi_{0.5}$ high-entropy alloy under different loads and sliding speeds. In a 90 wt% H_2O_2 environment, the coefficient of friction can be as low as 0.005–0.04, and the wear amount also decreases with the increase in sliding speed and the decrease in load, demonstrating the low wear characteristics of high-entropy alloys in an H_2O_2 environment. Duan et al. [86] analyzed the reasons for the reduced friction coefficient and smooth surface of the AlCoCrFeNiCu high-entropy alloy in a hydrogen peroxide environment, which were attributed to the combined effect of the protective film formed by oxidation products and the colloidal film. Luo et al. [87] analyzed the mechanism by which the tribological properties of the AlCoCrCuFeNi high-entropy alloy were affected at different heat treatment temperatures in a 90% hydrogen peroxide environment. As shown in Figure 14, with the increase in heat treatment temperature, the white flaky structure in the dendrite region (DR) of the high-entropy alloys increases, while the BCC phase decreases, resulting in a decrease in hardness. The decrease in hardness makes the material more easily penetrated

by abrasive particles in a hydrogen peroxide environment, and the coefficient of friction and wear increase accordingly. It indicates that in a strong oxidizing environment, material hardness is the key to resisting wear, and heat treatment affects hardness by changing the structure, thereby regulating the friction and wear performance.

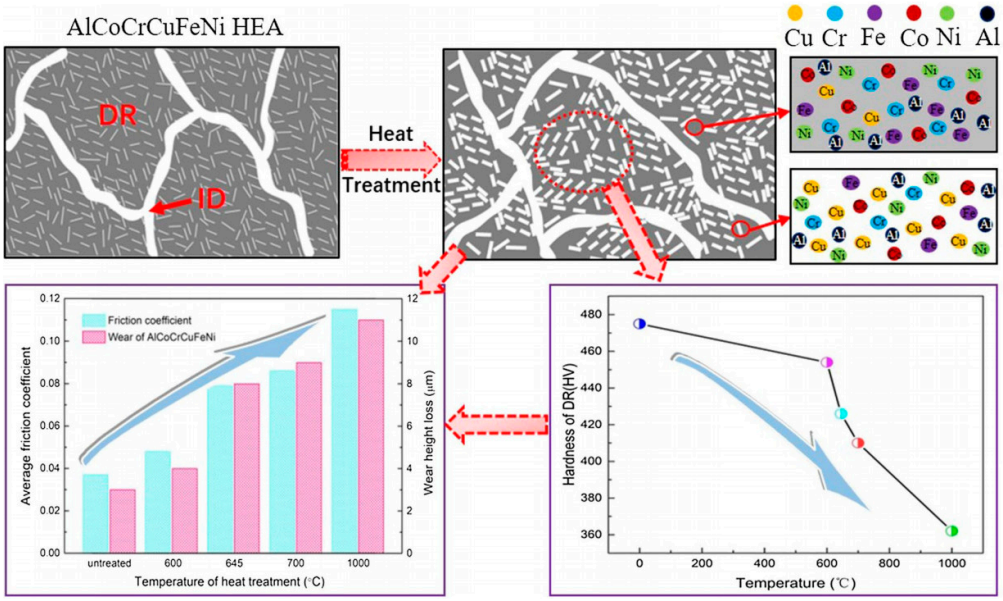


Figure 14. Mechanism analysis of tribological properties at different heat treatment temperatures [87].

This section systematically reviews the influence mechanisms of different friction environments on the friction and wear properties of high-entropy alloys. In high-temperature environments, the influence of temperature is complex. The wear resistance of some alloys increases with rising temperature. For instance, at 600 °C, $(CrMnFeHf)_{7.14}(TiTaV)_{23.81}$ has the best wear resistance. The friction coefficients of the laser cladding FeNiCoAlCu coating and the $Al_{0.25}$CoCrFeNi alloy both decrease with the increase in temperature. The lubrication and protection of the oxide film are key. In Marine environments, high-entropy alloys perform better than traditional alloys. Coatings such as $AlCrFeNiW_{0.2}Ti_{0.5}$ in seawater form a friction film containing $CaCO_3$ and Mg $(OH)_2$ through Ca^{2+} and Mg^{2+}, and combine with oxides generated by alloy elements to reduce friction and wear, demonstrating the composite protective mechanism of the friction film. In an H_2O_2 environment, high-entropy alloys can solve the compatibility problems of traditional metals. The friction and wear of $AlCoCrFeNiTi_{0.5}$, etc., improve with the increase in H_2O_2 concentration, and the colloid film and protective film play a key role. Heat treatment regulates performance by altering the structure and influencing hardness. The synergistic effect of material hardness and surface film is the core of optimization.

5. Influence of Test Conditions on the Tribological Properties of High-Entropy Alloys

High-entropy alloys exhibit broad application potential under diverse loading conditions, and their tribological properties show significant sensitivity to matching materials and the duration of wear tests. Different stress states (such as load magnitude and sliding rate) will change the frictional force between the friction pair and the alloy surface, thereby forming complex and variable wear surface morphologies, leading to corresponding changes in the friction coefficient and wear rate, and ultimately causing a transformation in the wear mechanism [88].

5.1. Load

Research shows that different loads will have a certain impact on the friction and wear of high-entropy alloys [89–91]. Joseph et al. [92] found that when studying the CoCrFeMnNi high-entropy alloy, there were significant differences in wear rates at room temperature, 600 °C, and 800 °C, with loads of 5 N and 10 N, respectively. At 600 °C, the lowest wear rate was observed under a 5 N load. This is attributed to the inhibitory effect of the subsurface ultrafine grain structure and σ relative grain boundary migration. In addition, the comparative tests of $(CoCrFeMnNi)_{85}Ti_{15}$ and CoCrFeMnNi under a load of 25 N and a rotational speed of 300 rpm show that the wear rate of the former is significantly lower than that of the latter due to its higher hardness. Deng et al.'s [93] research on the $CoCrFeNiMo_{0.2}$ high-entropy alloy shows that both the coefficient of friction and the wear rate decrease with the increase in normal load. This is because higher loads will promote the formation of a large amount of wear debris and oxide friction films on the surface. These substances hinder the direct contact of the friction pairs and, at the same time, reduce the interfacial contact stress. Tri et al. [94] found that at 500–600 °C, an increase in load from 10 N to 30 N led to an intensification of abrasive wear. Under a 30 N load, deeper furrows and more grinding debris appear, forming "three-body wear". The furrow phenomenon becomes more severe, and both the wear rate and the friction coefficient increase. Kumar et al. [95] conducted a study on $Al_{0.4}FeCrNiCo_x$. The results show that when the normal load increases from 5 N to 20 N, both the coefficient of friction and the specific wear rate gradually increase. This is because a higher load increases the direct contact area between metals, resulting in more wear chips and exacerbating surface damage. Lan et al. [96] investigated the tribological properties of $Ni_{45}(FeCoCr)_{40}(AlTi)_{15}$ high-entropy alloy under different normal loads. The research finds that the coefficient of friction decreases with the increase in load, and the coefficient of friction reaches the lowest value of 0.58 when the maximum load is 12 N. This is because the frictional heat generated in sliding contact increases with the increase in load, forming a thicker oxide layer. This oxide layer acts as an interfacial lubricant, reducing the shear strength and thereby reducing friction.

5.2. Sliding Velocity

The research shows that different sliding speeds also have a certain impact on the friction and wear of high-entropy alloys [97–102]. Studies have shown that the friction coefficient of $CoCrFeNiMo_{0.2}$ high-entropy alloy decreases with the increase in sliding speed, but the wear rate increases accordingly [93]. This is because when the sliding speed increases, the wear debris and oxide film formed on the surface decrease, which cannot effectively protect the surface, resulting in more furrows and plastic deformation during the friction process. Kumar et al.'s [95] study on $Al_{0.4}FeCrNiCo_x$ indicated that the wear rate decreased when the sliding speed increased from 0.5 m/s to 2 m/s. This is because the higher sliding speed causes the lubricating oil film to thicken, reducing direct metal contact. Kumar et al. [62] also studied the problems of $Al_{0.4}FeCrNiCo_x$ high-entropy alloy under dry friction conditions. The results show that the friction coefficient of the $Al_{0.4}FeCrNiCo_x$ high-entropy alloy decreases with the increase in speed. This is because high temperatures promote the formation of an oxide film, making the surface smoother. However, the specific wear rate increases with the increase in speed, as the high temperature without lubrication causes the material to soften, intensifying plastic deformation. Wu et al. [103] simulated and studied the influence of sliding speed on the friction behavior of the FeNiCrCoCu high-entropy alloy through nanomolecular dynamics software and found that sliding speed significantly affected the frictional force. There is an insignificant positive correlation between the two. However, as the speed increases,

the fluctuation range of the frictional force expands, which is related to the fact that the alloy releases more strain energy under a specific pressure. Qiu et al. [104] also studied the friction and wear properties of the FeNiCrCoCu high-entropy alloy using the same molecular dynamics method. The influence of cutting speed is explored by analyzing the coefficient of friction, stress distribution and dislocations. It was found that an increase in speed would increase the tangential force, but had a small effect on the normal force, and made the high-temperature area more obvious during the friction process.

5.3. Friction Pair

The friction pair can also have a certain impact on the friction and wear of high-entropy alloys [105–107]. Miao et al. [108] investigated the friction behavior of the $AlCoCrFeNi_{2.1}$ high-entropy alloy with different friction pairs. The results show that the friction coefficient and wear rate vary significantly due to different friction pairs. When paired with SiC, $AlCoCrFeNi_{2.1}$ has the lowest coefficient of friction and the smallest wear rate. When $AlCoCrFeNi_{2.1}$ is paired with Al_2O_3, it has the highest coefficient of friction and the most severe wear. The research shows [109] that when $CrFeCo_{1.5}Ni_{1.5}Ti_{0.5}$ is paired with Al_2O_3 balls, severe delamination wear occurs due to the high hardness of the ceramics. When $CrFeCo_{1.5}Ni_{1.5}Ti_{0.5}$ is paired with 100Cr6 steel balls, the oxide film on the surface of the steel balls reduces friction, and the amount of wear is significantly reduced. At this point, slight oxidation wear is predominant. A comparison between $CrFeCo_{1.5}Ni_{1.5}Ti_{0.5}$ and Inconel 718 reveals that the wear rate of high-entropy alloys when paired with steel balls is lower. This indicates that it has more advantages in the balance between lightweight and wear resistance. When $Al_xCoCrFeNi$ is paired with Inconel 718 friction pairs, at a high temperature of 800 °C, due to the formation of an oxide layer on the surface of Inconel 718, the friction coefficient drops to 0.35, and the wear mechanism is mainly oxidative wear [110]. When CoCrFeMnNi is paired with Si_3N_4 balls, the SiO_2 layer formed by Si_3N_4 during sliding acts as a lubricant, reducing the wear rate by approximately 30% [72]. Poulia et al. found [111] that the wear rate of the MoTaNbZrTi high-entropy alloy when paired with 100Cr6 steel balls was lower than that when paired with Al_2O_3 ceramic balls. This is because the oxide film formed on the surface of the steel ball during friction can play a lubricating role, while the high hardness of ceramics will have a more severe ploughing effect on the surface of the alloy.

In the test conditions, the load, sliding speed and friction pair have a significant impact on the friction and wear performance of high-entropy alloys. In terms of load, different alloys respond differently. For some, due to the reduced contact caused by the surface oxide film, the friction coefficient and wear rate decrease with the increase in load. Some others increase due to the increase in contact area and the intensification of abrasive wear, both of which rise with the increase in load. The influence of sliding speed is complex. By altering the oxide film, oil film and the degree of material softening, it leads to changes in the coefficient of friction and wear rate, and also affects the fluctuation of frictional force. The compatibility of the friction pair has a significant impact. When paired with different materials, the friction coefficient and wear rate vary significantly, which is related to the hardness of the friction pair, the oxide film and the lubrication effect. Reasonable selection can optimize wear resistance.

6. Conclusions

High-entropy alloys have demonstrated significant advantages in the field of friction and wear due to the synergistic effect of the four core effects. The research shows that metallic elements (such as Al, Ti, Cu, etc.) can effectively regulate their friction and wear properties through solid solution strengthening, second-phase precipitation and oxide film

formation, while non-metallic elements (such as C, Si, etc.) can form strengthening phases. High temperature, marine conditions, hydrogen peroxide and other working environments affect its tribological behavior by altering the wear mechanism. Friction schemes such as load, sliding velocity and friction pair have an impact on the performance of high-entropy alloys. The coefficient of friction and wear rate vary under different conditions. Reasonable matching can optimize wear resistance. Based on this, high-entropy alloys have application potential in specific components such as engine blades and bearings in the aerospace field, impellers of seawater pumps and ship propellers in the Marine engineering field, as well as brake discs of high-speed trains and piston rings of automobiles in the mechanical manufacturing field.

Author Contributions: Conceptualization, S.Z.; Data curation, W.L. and H.G.; Methodology, S.Z.; Writing—original draft, S.Z.; Writing—review and editing, Z.W.; Funding acquisition, S.Z. All authors have read and agreed to the published version of the manuscript.

Funding: This work was supported by the General Project of Natural Science Foundation of Liaoning Province (2025-MS-309), the Scientific Research Project of the Education Department of Liaoning Province (LJ212513217002) and the Research Funding of Talent Introduction Program of Liaoning Technical University (552305900128).

Conflicts of Interest: The authors declare no conflicts of interest.

References

1. Liu, M.; Xu, L.; Zhu, C.; Li, Z.; Wei, S. Research progress of high entropy alloy: Surface treatment improves friction and wear properties. *J. Mater. Res. Technol.* **2024**, *28*, 752–773. [CrossRef]
2. Goud, D.; Sarkar, M.; Kopperi, H.; Das, A.; Ray, B.; Vijayaraghavan, S.; Pathak, B.; Peter, S.C. High entropy alloy formation derived from high entropy oxide: Unlocking the active sites for green methanol production from CO_2. *Adv. Mater.* **2025**, *37*, 2504180. [CrossRef]
3. Kim, K.S.; Couillard, M.; Tang, Z.; Shin, H.; Poitras, D.; Cheng, C.; Naboka, O. Continuous synthesis of high-entropy alloy nanoparticles by in-flight alloying of elemental metals. *Nat. Commun.* **2024**, *15*, 1450. [CrossRef]
4. Li, T.X.; Wang, S.D.; Lu, Y.P.; Cao, Z.Q.; Wang, T.M.; Li, T.J. Research progress and prospect of high-entropy alloy materials. *Chin. Eng. Sci.* **2023**, *25*, 170–181. [CrossRef]
5. Holmberg, K.; Andersson, P.; Erdemir, A. Global energy consumption due to friction in passenger cars. *Tribol. Int.* **2012**, *47*, 221–234. [CrossRef]
6. Oketola, A.M.; Adegbola, T.A.; Jamiru, T.; Ogunbiyi, O.; Salifu, S. Advances in high-entropy alloy research: Unraveling fabrication techniques, microstructural transformations, and mechanical properties. *J. Bio-Tribo-Corros.* **2025**, *11*, 22–29. [CrossRef]
7. Miguel, L.J.M.; Ileana, M.M.; Victor, G.; Ionelia, V. New FeMoTaTiZr high-entropy alloy for medical applications. *Metals* **2025**, *15*, 259. [CrossRef]
8. Lim, X.Z. Mixed-up metals make for stronger, tougher, stretchier alloys. *Nature* **2016**, *533*, 306–307. [CrossRef]
9. Cantor, B.; Chang, I.T.H.; Knight, P. Microstructural development in equiatomic multicomponent alloys. *Mater. Sci. Eng. A* **2004**, *375*, 213–218. [CrossRef]
10. Tsai, M.H.; Yeh, J.W. High-Entropy Alloys: A Critical Review. *Mater. Res. Lett.* **2014**, *2*, 107–123. [CrossRef]
11. Yeh, J.W. Alloy design strategies and future trends in high-entropy alloys. *J. Mater. Metall. Mater. Soc.* **2013**, *65*, 1759–1771. [CrossRef]
12. Zhang, Y.; Zuo, T.T.; Tang, Z.; Gao, M.C.; Dahmen, K.A.; Liaw, P.K.; Lu, Z.P. Microstructures and properties of high-entropy alloys. *Prog. Mater. Sci.* **2014**, *61*, 1–93. [CrossRef]
13. Yeh, J.W.; Chen, Y.L.; Lin, S.J.; Chen, S.K. High-Entropy Alloys-A New Era of Exploitation. *Mater. Sci. Forum* **2007**, *560*, 1–9. [CrossRef]
14. Yeh, J.W.; Chen, S.K.; Lin, S.J.; Gan, J.Y.; Chin, T.S.; Shun, T.T.; Tsau, C.H.; Chang, S.Y. Nanostructured high-entropy alloys with multiple principalelements novel alloy design concepts and outcomes. *Adv. Eng. Mater.* **2004**, *6*, 299–303. [CrossRef]
15. Yeh, J.W.; Su, J.L.; Chin, T.S.; Gan, J.Y.; Chen, S.W.; Shun, T.T.; Tsau, C.H.; Chou, S.Y. Formation of simple crystal structures in Cu-Co-Ni-Cr-Al-Fe-Ti-Valloys with multiprincipal metallic elements. *Metall. Mater. Trans. A* **2004**, *35*, 2533–2536. [CrossRef]
16. Shi, P.J.; Li, R.G.; Li, Y.; Wen, Y.B.; Zhong, Y.B.; Ren, W.L.; Shen, Z.; Zheng, T.X.; Peng, J.C.; Liang, X.L.; et al. Hierarchical crack buffering triples ductility in eutectic herringbone high-entropy alloys. *Science* **2021**, *373*, 912–918. [CrossRef] [PubMed]

17. Ding, J.; Asta, M.; Ritchie, R.O. Melts of CrCoNi-based high-entropy alloys: Atomic diffusion andelectronic/atomic structure from ab initio simulation. *Appl. Phys. Lett.* **2018**, *113*, 111902. [CrossRef]
18. Coury, F.G.; Butler, T.; Chaput, K.; Saville, A.; Copley, J.; Foltz, J.; Mason, P.; Clarke, K.; Kaufman, M.; Clarke, A. Phase equilibria, mechanical properties and design of quaternary refractory high entropy alloys. *Mater. Des.* **2018**, *155*, 244–256. [CrossRef]
19. Sharma, P.; Dwivedi, V.K.; Dwivedi, S.P. Development of high entropy alloys: A review. *Mater. Today* **2021**, *43*, 502–509. [CrossRef]
20. Liao, M.Q.; Liu, Y.; Min, L.J.; Lai, Z.H.; Han, T.Y.; Yang, D.N.; Zhu, J.C. Alloying effect on phase stability, elastic and thermodynamic properties of Nb-Ti-V-Zr high entropy alloy. *Intermetallics* **2018**, *101*, 152–164. [CrossRef]
21. Wei, Q.Q.; Shen, Q.; Zhang, J.; Chen, B.; Luo, G.Q.; Zhang, L.M. Microstructure and mechanical property of a novel ReMoTaW high-entropy alloy with high density. *Int. J. Refract. Meth.* **2018**, *77*, 8–11. [CrossRef]
22. Ikeuchi, D.; King, D.J.M.; Laws, K.J.; Knowles, A.J.; Aughterson, R.D.; Lumpkin, G.R.; Obbard, E.G. Cr-Mo-V-W: A new refractory and transition metalhigh-entropy alloy system. *Scripta. Mater.* **2019**, *158*, 141–145. [CrossRef]
23. Chaudhary, V.; Gwalani, B.; Soni, V.; Ramanujan, R.V.; Banerjee, R. Influence of Cr substitution and temperature on hierarchical-phase decomposition in the AlCoFeNi high entropy alloy. *Sci. Rep.* **2018**, *8*, 15578. [CrossRef]
24. Yeh, J.W. Recent progress in high entropy alloys. *Ann. Chim. Sci. Mat.* **2006**, *31*, 633–648. [CrossRef]
25. Ng, C.; Guo, S.; Luan, J.; Shi, S.; Liu, C.T. Entropy-driven phase stability and slow diffusion kinetics in an $Al_{0.5}$CoCrCuFeNi high entropy alloy. *Intermetallics* **2012**, *31*, 165–171. [CrossRef]
26. Li, A.; Zhang, X. Thermodynamic analysis of the simple microstructure of AlCrFeNiCu high-entropy alloy with multi-principal elements. *Acta Metall. Sin.* **2009**, *22*, 219–224. [CrossRef]
27. Tong, C.J.; Chen, Y.L.; Chen, S.K. Microstructure characterization of Al_xCoCrCuFeNi high-entropy alloy system with multiprincipal elements. *Metall. Mater. Trans. A* **2005**, *36*, 881–893. [CrossRef]
28. Tong, C.J.; Chen, M.R.; Chen, S.K. Mechanical performance of the Al_xCoCrCuFeNi high-entropy alloy system with multiprincipal elements. *Metall. Mater. Trans. A* **2005**, *36*, 1263–1271. [CrossRef]
29. Lucas, M.S.; Wilks, G.B.; Mauger, L.; Munoz, J.A.; Karapetrova, E. Absence of long-range chemical ordering in equimola FeCoCrNi. *Appl. Phys. Lett.* **2012**, *100*, 251907. [CrossRef]
30. Senkov, O.N.; Wilks, G.B.; Miracle, D.B.; Chuang, P.C.; Liaw, P.K. Refractory high-entropy alloys. *Intermetallics* **2010**, *18*, 1758–1765. [CrossRef]
31. Del, G.M.F.; Bozzolo, G.; Hugo, O.M. Determination of the transition to the high entropy regime for alloys of refractory elements. *J. Alloy. Compd.* **2012**, *534*, 25–31. [CrossRef]
32. Inoue, A. Stabilization of metallic supercooled liquid and bulk amorphous alloys. *Acta Mater.* **2000**, *48*, 279–306. [CrossRef]
33. Yeh, J.W.; Chang, S.Y.; Hong, Y.D.; Chen, S.K.; Lin, S.J. Anomalous decrease in X-ray diffraction intensities of CuNiAlCoCrFeSi alloy systems with multi-principal elements. *Mater. Chem. Phys.* **2007**, *103*, 41–46. [CrossRef]
34. Wang, Z.F.; Zhang, S. Research and application progress of high-entropy alloys. *Coatings* **2023**, *13*, 1916. [CrossRef]
35. Tsai, M.H. Physical Properties of high entropy alloys. *Entropy* **2013**, *15*, 5338–5345. [CrossRef]
36. Chen, W.Y.; Liu, X.; Chen, Y.R.; Yeh, J.W.; Tseng, K.K.; Natesan, K. Irradiation effects in high entropy alloys and 316H stainless steel at 300 degrees C. *J. Nucl. Mater.* **2018**, *510*, 421–430. [CrossRef]
37. Kucza, W.; Dabrowa, J.; Danielewski, M.; Kulik, T.; Cieslak, G. Interdiffusion in the FCC-structured Al-Co-Cr-Fe-Ni high entropy alloys: Experimental studies and numerical simulations. *J. Alloy. Compd.* **2016**, *674*, 455–462. [CrossRef]
38. Vaidya, M.; Trubel, S.; Murty, B.S.; Wilde, G.; Divinski, S.V. Ni tracer diffusion in CoCrFeNi and CoCrFeMnNi highentropy alloys. *J. Alloy. Compd.* **2016**, *688*, 994–1001. [CrossRef]
39. Yang, M.; Liu, X.J.; Ruan, H.H.; Wu, Y.; Wang, H.; Lu, Z.P. High thermal stability and sluggish crystallization kinetics of high-entropy bulk metallic glasses. *J. Appl. Phys.* **2016**, *119*, 1–7. [CrossRef]
40. Wang, R.; Chen, W.M.; Zhong, J.; Zhang, L. Experimental and numerical studies on the sluggish diffusion in face centered cubic Co-Cr-Cu-Fe-Ni high-entropy alloys. *J. Mater. Sci. Technol.* **2018**, *34*, 1791–1798. [CrossRef]
41. Kottke, J.; Laurent-Brocq, M.; Fareed, A.; Wilde, G. Tracer diffusion in the Ni-CoCrFeMn system: Transitionfrom a dilute solid solution to a high entropy alloy. *Scripta Mater.* **2019**, *159*, 94–98. [CrossRef]
42. Tsai, K.Y.; Tsai, M.H.; Yeh, J.W. Sluggish diffusion in Co–Cr–Fe–Mn–Ni high-entropy alloys. *Acta Mater.* **2013**, *61*, 4887–4897. [CrossRef]
43. Praveen, S.; Kim, H.S. High-entropy alloys: Potential candidates for high-temperature applications–an overview. *Adv. Eng. Mater.* **2018**, *20*, 1700645. [CrossRef]
44. Xu, Z.X.; Song, H.; Li, P.J.; Zhu, X.; Zhang, S.; Wang, Q.; Duan, P.G.; Hu, X. A new method for removal of nitrogen in sewage sludge-derived hydrochar with hydrotalcite as the catalyst. *J. Hazard. Mater.* **2020**, *398*, 122833. [CrossRef] [PubMed]
45. Ranganathan, S. Alloyed pleasures: Multimetallic cocktails. *Curr. Sci.* **2003**, *85*, 1404–1406. [CrossRef]
46. Sanchez, J.M.; Vicario, I.; Albizuri, J.; Guraya, T.; Garcia, J.C. Phase prediction, microstructure and high hardness of novel light-weight high entropy alloys. *J. Mater. Res. Technol.* **2019**, *8*, 795–803. [CrossRef]

47. Huang, D.; Lu, J.; Zhuang, Y.; Tian, C.; Li, Y. The role of Nb on the high temperature oxidation behavior of $CoCrFeMnNb_xNi$ high-entropy alloys. *Corros. Sci.* **2019**, *158*, 108088.1–108088.9. [CrossRef]
48. Cao, B.X.; Wang, C.; Yang, T.; Liu, C.T. Cocktail effects in understanding the stability and properties of face-centered-cubic high-entropy alloys at ambient and cryogenic temperatures. *Scr. Mater.* **2020**, *187*, 250–255. [CrossRef]
49. Gwalani, B.; Choudhuri, D.; Soni, V.; Ren, Y.; Styles, M.; Hwang, J.Y.; Nam, S.J.; Ryu, H.; Hong, S.H.; Banerjee, R. Cu assisted stabilization and nucleation of L12 precipitates in Al0.3CuFeCrNi2fcc-based high entropy alloy. *Acta Mater.* **2017**, *129*, 170–182. [CrossRef]
50. Pickering, E.J.; Jones, N.G. High-entropy alloys: A critical assessment of their founding principles and future prospects. *Int. Mater. Rev.* **2016**, *61*, 183–202. [CrossRef]
51. Kumar, A.; Singh, A.; Suhane, A. Mechanically alloyed high entropy alloys: Existing challenges and opportunities. *J. Mater. Res. Technol.* **2022**, *17*, 2431–2456. [CrossRef]
52. Wu, J.M.; Lin, S.J.; Yeh, J.W.; Chen, S.K.; Chen, H.C. Adhesive wear behavior of AlxCoCrCuFeNi high-entropy alloys as a function of aluminum content. *Wear* **2006**, *261*, 513–519. [CrossRef]
53. Li, G.; Wen, Y.; Yu, Z.M.; Liu, J.; Xiong, Z.L. Effect of Al content on properties of CrFeNiAlxSi high entropy alloy. *Chin. J. Mater. Res.* **2021**, *35*, 712–720. [CrossRef]
54. Cheng, H.; Fang, Y.; Xu, J.; Zhu, C.; Xue, S. Tribological properties of nano/ultrafine-grained fecocrnimnalx high-entropy alloys over a wide range of temperatures. *J. Alloys Compd.* **2019**, *817*, 153305. [CrossRef]
55. Wang, J.Y.; Zhang, B.S.; Yu, Y.Q.; Zhang, Z.J.; Zhu, S.S.; Lou, X.; Wang, Z.Z. Study of high temperature friction and wear performance of $(CoCrFeMnNi)_{85}Ti_{15}$ high-entropy alloy coating prepared by plasma cladding. *Surf. Coatings Technol.* **2020**, *384*, 125337. [CrossRef]
56. Ye, H.M.; Zhan, Y.Z.; Nie, N. Development of novel $CoCu_{0.5}FeNiVTi_x$ (x = 0.5, 1, 1.5, 2) high-entropy alloys. *Mater. Sci. Technol.* **2017**, *4*, 952–960. [CrossRef]
57. Xu, Z.; Li, D.Y.; Chen, D.L. Effect of Ti on the wear behavior of AlCoCrFeNi high-entropy alloy during unidirectional and bi-directional sliding wear processes. *Wear* **2021**, *476*, 203650. [CrossRef]
58. Mukanov, S.; Loginov, P.; Fedotov, A.; Bychkova, M.; Antonyuk, M.; Levashov, E. The effect of copper on the microstructure, wear and corrosion resistance of CoCrCuFeNi high-entropy alloys manufactured by powder metallurgy. *Materials* **2023**, *16*, 1178. [CrossRef]
59. Verma, A.; Tarate, P.; Abhyankar, A.C.; Mohape, M.R.; Gowtam, D.S.; Deshmukh, V.P.; Shanmugasundaram, T. High temperature wear in CoCrFeNiCux high entropy alloys: The role of Cu. *Scr. Mater.* **2019**, *161*, 28–31. [CrossRef]
60. Hsu, C.Y.; Sheu, T.S.; Yeh, J.W.; Chen, S.K. Effect of iron content on wear behavior of $AlCoCrFexMo_{0.5}Ni$ high-entropy alloys. *Wear* **2010**, *268*, 653–659. [CrossRef]
61. Shu, F.; Yang, B.; Dong, S.; Zhao, H.Y.; Xu, B.S.; Xu, F.J.; Liu, B.; He, P.; Feng, J.C. Effects of Fe-to-Co ratio on microstructure and mechanical properties of laser cladded FeCoCrBNiSi high-entropy alloy coatings. *Appl. Surf. Sci.* **2018**, *450*, 538–544. [CrossRef]
62. Kumar, S.; Patnaik, A.; Pradhan, A.K.; Kumar, V. Dry sliding wear behavior of $Al_{0.4}FeCrNiCo_x$(x = 0, 0.25, 0.5, 1.0 mol) high-entropy alloys. *Metallogr. Microstruct. Anal.* **2019**, *8*, 545–557. [CrossRef]
63. Cheng, J.B.; Liang, X.B.; Xu, B.S. Effect of Nb addition on the structure and mechanical behaviors of CoCrCuFeNi high-entropy alloy coatings. *Surf. Coat. Technol.* **2014**, *240*, 184–190. [CrossRef]
64. Yu, Y.; He, F.; Qiao, Z.; Wang, Z.; Liu, W.; Yang, J. Effects of temperature and microstructure on the triblogical properties of cocrfeninbx eutectic high entropy alloys. *J. Alloy. Compd.* **2019**, *775*, 1376–1385. [CrossRef]
65. Liu, Y.; Zhang, F.; Huang, Z.; Zhou, Q.; Ren, Y.; Du, Y.; Wang, H. Mechanical and dry sliding tribological properties of CoCrNiNb medium-entropy alloys at room temperature. *Tribol. Int.* **2021**, *163*, 107160. [CrossRef]
66. Deng, G.Y.; Tieu, A.K.; Su, L.H.; Wang, P.; Wang, L.; Lan, X.D.; Cui, S.G.; Zhu, H.T. Investigation into reciprocating dry sliding friction and wear properties of bulk CoCrFeNiMo high entropy alloys fabricated by spark plasma sintering and subsequent cold rolling processes:role of Mo element concentration. *Wear* **2020**, *460*, 203440. [CrossRef]
67. Chen, B.; Li, X.M.; Chen, W.J.; Shang, L.; Jia, L.M. Microstructural evolution, mechanical and wear properties, and corrosion resistance of as-cast CrFeNbTiMox refractory high entropy alloys. *Intermetallics* **2023**, *155*, 107829. [CrossRef]
68. Wang, S.W.; Zhou, H.; Xu, Y.G.; Zhang, K.F.; Feng, K. Tribological properties of $CoCrFeNiW_x$ high-entropy alloys at room temperature and 900 °C. *Tribology* **2024**, *44*, 312–322. [CrossRef]
69. Xiao, J.K.; Tan, H.; Chen, J.; Martini, A.; Zhang, C. Effect of carbon content on microstructure, hardness and wear resistance of CoCrFeMnNiCx high-entropy alloys. *J. Alloy. Compd.* **2020**, *847*, 156533. [CrossRef]
70. Jin, B.Q.; Zhang, N.N.; Wang, F.Z.; Zhang, Y.; Li, D.Y. Phase evolution and wear mechanism of $AlCoCrFeNiSi_x$ high-entropy alloys produced by arc melting. *Mater. Res. Express* **2018**, *5*, 096505. [CrossRef]
71. Kumar, A.; Swarnakar, A.K.; Basu, A.; Chopkar, M. Effects of processing route on phase evolution and mechanical properties of $CoCrCuFeNiSi_x$ high entropy alloys. *J. Alloy. Compd.* **2018**, *748*, 889–897. [CrossRef]

72. Xin, B.B.; Zhang, A.J.; Han, J.S.; Meng, J.H. Improving mechanical properties and tribological performance of $Al_{0.2}Co_{1.5}CrFeNi_{1.5}Ti_{0.5}$ high entropy alloys via doping Si. *J. Alloy. Compd.* **2021**, *869*, 159122. [CrossRef]
73. Liu, X.T.; Lei, W.B.; Ma, L.J.; Liu, J.L.; Liu, J.; Cui, J.Z. Effect of boron on the microstructure, phase assemblage and wear properties of $Al_{0.5}CoCrCuFeNi$ high-entropy alloy. *Rare Met. Mater. Eng.* **2016**, *45*, 2201–2207. [CrossRef]
74. Lin, D.Y.; Zhang, N.N.; He, B. Tribological properties of FeCoCrNiAlB-x high-entropy alloys coating prepared by lasercladding. *J. Iron Steel Res. Int.* **2017**, *24*, 184–189. [CrossRef]
75. Wang, Z.F.; Zhang, S. Research progress of laser cladding coating on titanium alloy surface. *Coatings* **2024**, *14*, 1495. [CrossRef]
76. Hamdi, H.; Abedi, H.R.; Zhang, Y. A study on outstanding high-temperature wear resistance of high-entropy alloys. *Adv. Eng. Mater.* **2023**, *25*, 2201915. [CrossRef]
77. Kumar, D. Recent advances in tribology of high entropy alloys: A critical review. *Prog. Mater. Sci.* **2023**, *136*, 101106. [CrossRef]
78. Wu, J.; Chen, Y.; Zhu, H.G. A review on the tribological performances of high-entropy alloys. *Adv. Eng. Mater.* **2022**, *24*, 2101548. [CrossRef]
79. Xing, Q.W.; Feltrin, A.C.; Akhtar, F. Processing, microstructure and high temperature dry sliding wear of a Cr-Fe-Hf-Mn-Ti-Ta-V high-entropy alloy based composite. *Mater. Today Commun.* **2021**, *28*, 102657. [CrossRef]
80. Jin, G.; Cai, Z.B.; Guan, Y.J.; Cui, X.; Liu, Z.; Li, Y.; Dong, M.L.; Zhang, D. High temperature wear performance of laser-cladded FeNiCoAlCu high-entropy alloy coating. *Appl. Surf. Sci.* **2018**, *445*, 113–122. [CrossRef]
81. Du, L.M.; Lan, L.W.; Zhu, S.; Yang, H.J.; Shi, X.H.; Liaw, P.K.; Qiao, J.W. Effects of temperature on the tribological behavior of Al_(0.25)CoCrFeNi high-entropy alloy. *J. Mater. Sci. Technol.* **2019**, *35*, 217–225. [CrossRef]
82. Liang, H.; Qiao, D.; Miao, J.; Cao, Z.; Wang, T. Anomalous microstructure and tribological evaluation of $AlCrFeNiW_{0.2}Ti_{0.5}$ high-entropy alloy coating manufactured by laser cladding in seawater. *J. Mater. Sci. Technol.* **2021**, *85*, 224–234. [CrossRef]
83. Liang, H.; Miao, J.W.; Gao, B.Y.; Deng, D.W.; Wang, T.M.; Lu, Y.P.; Cao, Z.Q.; Jiang, H.; Li, T.J.; Kang, H.J. Microstructure and tribological properties of $AlCrFe_2Ni_2W_{0.2}Mo_{0.75}$ high-entropy alloy coating prepared by laser cladding in seawater, NaCl solution and deionized water. *Surf. Coat. Technol.* **2020**, *400*, 126214. [CrossRef]
84. Yu, Y.J.; Wang, J.; Yang, J.; Qiao, Z.H.; Duan, H.T.; Li, J.S.; Li, J.; Liu, W.M. Corrosive and tribological behaviors of AlCoCrFeNi-M high entropy alloys under 90 wt. % H_2O_2 solution. *Tribol. Int.* **2019**, *131*, 24–32. [CrossRef]
85. Yuan, Y.; Xin, Y.L.; Hai, T.D.; Jun, Y.; Zhu, H.Q.; Jian, L.; Jin, S.L. Outstanding self-lubrication of SiC ceramic with porous surface/$AlCoCrFeNiTi_{0.5}$ high-entropy alloy tribol-pair under 90wt% H_2O_2 harsh environment. *Mater. Lett.* **2020**, *276*, 128025. [CrossRef]
86. Duan, H.T.; Wu, Y.; Hua, M.; Yuan, C.Q.; Wang, D.; Tu, J.S.; Kou, H.C.; Li, J. Tribological properties of AlCoCrFeNiCu high-entropy alloy in hydrogen peroxide solution and in oil lubricant. *Wear* **2013**, *297*, 1045–1051. [CrossRef]
87. Luo, X.S.; Li, J.; Jin, Y.L.; Hu, C.P.; Jia, D.; Zhan, S.P.; Yu, Y.; Hua, M.; Duan, H.T. Heat treatment influence on tribological properties of AlCoCrCuFeNi high-entropy alloy in Hydrogen Peroxide-Solution. *Met. Mater. Int.* **2020**, *26*, 1286. [CrossRef]
88. Zirari, T.; Trabadelo, V. A review on wear, corrosion, and wear-corrosion synergy of high entropy alloys. *Heliyon* **2024**, *10*, e25867. [CrossRef]
89. Cheenepalli, N.; You, H.J.; Suseong, A.; Song, J.W.; Jeong, K.Y.; Madavali, B.B.; Gian, S.; Na, Y.S.; Jong, W.W.; Kim, H.S.; et al. Worn surface and subsurface layer structure formation behavioron wear mechanism of CoCrFeMnNi high entropy alloy in different sliding conditions. *Appl. Surf. Sci.* **2021**, *549*, 149202. [CrossRef]
90. Yu, Y.; Wang, J.; Li, J.S.; Kou, H.C.; Niu, S.Z.; Zhu, S.Y.; Yang, J.; Liu, W.M. Dry-sliding tribological properties of $AlCoCrFeNiTi_{0.5}$ high-entropy alloy. *Rare Met.* **2022**, *41*, 4266. [CrossRef]
91. Wang, Y.; Li, D.; Yang, J.S.; Jin, J.S.; Zhang, M.; Wang, X.Y.; Li, B.; Hu, Z.G.; Gong, P. Effect of grain size on the tribological behavior of CoCrFeMnNi high entropy alloy. *Materials* **2023**, *16*, 1714. [CrossRef]
92. Joseph, J.; Haghdadi, N.; Annasamy, M.; Kada, S.R.; Fabijanic, D. On the enhanced wear resistance of CoCrFeMnNi high entropy alloy at intermediate temperature. *Scr. Mater.* **2020**, *186*, 230–235. [CrossRef]
93. Deng, G.Y.; Tieu, A.K.; Lan, X.D.; Su, L.H.; Wang, L.; Zhu, Q.; Zhu, H.T. Effects of normal load and velocity on the dry sliding tribological behaviour of $CoCrFeNiMo_{0.2}$ high entropy alloy. *Tribol. Int.* **2020**, *144*, 106116. [CrossRef]
94. Vo, T.D.; Tran, B.; Tieu, A.K.; Wexler, D.; Deng, G.Y.; Nguyen, C. Effects of oxidation on friction and wear properties of eutectic high-entropy alloy $AlCoCrFeNi_{2.1}$. *Tribol. Int.* **2021**, *160*, 107017. [CrossRef]
95. Kumar, S.; Patnaik, A.; Pradhan, A.K.; Kumar, V. Room temperature wear study of $Al_{0.4}FeCrNiCo_x$ (x = 0, 0.25, 0.5, 1.0 mol) high-entropy alloys under oil lubricating conditions. *J. Mater. Res.* **2019**, *34*, 841–853. [CrossRef]
96. Lan, L.W.; Wang, X.J.; Guo, R.P.; Yang, H.J.; Qiao, J.W. Effect of environments and normal loads on tribological properties of nitrided $Ni_{45}(FeCoCr)_{40}(AlTi)_{15}$ high-entropy alloys. *J. Mater. Sci. Technol.* **2020**, *42*, 85–96. [CrossRef]
97. Firstov, S.A.; Gorban, V.F.; Krapivka, N.A.; Karpets, M.V.; Kostenko, A.D. Wear resistance of high-entropy alloys, Powder Metall. *Met. Ceram.* **2017**, *56*, 158–164. [CrossRef]
98. Ren, Y.; Jia, Q.; Du, Y.; Zhou, Q.; Greiner, C.; Hua, K.; Wang, H.F.; Wang, J. A wear-resistant metastable CoCrNiCu high-entropy alloy with modulated surface and subsurface structures. *Friction* **2022**, *10*, 1722–1738. [CrossRef]

99. Li, Y.; Liang, H.; Nie, Q.; Qi, Z.; Cao, Z. Microstructures and wear resistance of $CoCrFeNi_2V_{0.5}Ti_x$ high-entropy alloy coatings prepared by laser cladding. *Crystals* **2020**, *10*, 352. [CrossRef]
100. Li, J.Y.; Dong, L.G.; Dong, X.W.; Zhao, W.H.; Liu, J.H.; Xiong, J.X.; Xu, C.Y. Study on wear behavior of FeNiCrCoCu high entropy alloy coating on Cu substrate based on molecular dynamics. *Appl. Surf. Sci.* **2021**, *570*, 151236. [CrossRef]
101. Wang, H.; Ren, K.; Xie, J.; Zhang, C.; Tang, W.C. Friction and wear behavior of single-phase high-entropy alloy FeCoNiCrMnunderMoS_2-oil lubrication. *Ind. Lubr. Tribol.* **2019**, *72*, 665–672. [CrossRef]
102. Zhang, Y.; Han, T.; Xiao, M.; Shen, Y. Effect of iron content on microstructure and properties of $Fe_xNi_2Co_2CrTiNb$ high-entropy alloy coating. *Optik* **2020**, *204*, 164168. [CrossRef]
103. Wu, Y.L.; Tan, J.; Li, X.M.; Qiu, Z.J.; Zhang, R.Z. Molecular dynamics study on friction of high-entropy alloy FeNiCrCoCu. *Mater. Today Commun.* **2023**, *37*, 107107. [CrossRef]
104. Qiu, J.Z.; Xu, Z.H.; Song, J.R.; Hu, C.X.; Miao, L.L.; He, X.D. Molecular dynamics simulation of a new inhomogeneous concentration distribution model based on frictional behavior of FeNiCrCoCu high-entropy alloy. *Mater. Today Commun.* **2023**, *35*, 106337. [CrossRef]
105. Yu, Y.; Wang, J.; Li, J.S.; Kou, H.C.; Duan, H.T.; Li, J.; Liu, W.M. Tribological behavior of AlCoCrCuFeNi and $AlCoCrFeNiTi_{0.5}$ high entropy alloys under hydrogen peroxide solution against different counterparts. *Tribol. Int.* **2015**, *92*, 203–210. [CrossRef]
106. Anthoula, P.; Emmanuel, G.; Angela, L.; Alexander, K. Dry-sliding wear response of MoTaWNbV high entropy alloy. *Adv. Eng. Mater.* **2017**, *19*, 1600535. [CrossRef]
107. Li, X.; Feng, Y.; Liu, B.; Yi, D.; Yang, X.; Zhang, W.; Chen, G.; Liu, Y.; Bai, P. Influence of NbC particles on microstructure and mechanical properties of AlCoCrFeNi high-entropy alloy coatings prepared by laser cladding. *J. Alloy. Compd.* **2019**, *788*, 485–494. [CrossRef]
108. Miao, J.; Liang, H.; Zhang, A.; He, J.; Meng, J.; Lu, Y. Tribological behavior of an $AlCoCrFeNi_{2.1}$ eutectic high entropy alloy sliding against different counterfaces. *Tribol. Int.* **2021**, *153*, 106599. [CrossRef]
109. Lentzaris, K.; Poulia, A.; Georgatis, E.; Lekatou, A.G.; Karantzalis, A.E. Analysis of microstructure and sliding wear behavior of $Co_{1.5}CrFeNi_{1.5}Ti_{0.5}$ High-Entropy Alloy. *J. Mater. Eng. Perform.* **2018**, *27*, 5177–5186. [CrossRef]
110. Lu, S.; Zhou, J.; Wang, L.; Liang, J. Influence of $MoSi_2$ on the microstructure and elevated-temperature wear properties of Inconel 718 coating fabricated by laser cladding. *Surf. Coat. Technol.* **2021**, *424*, 127665. [CrossRef]
111. Mathiou, C.; Poulia, A.; Georgatis, E.; Karantzalis, A.E. Microstructural features and dry—Sliding wear response of MoTaNbZrTi high entropy alloy. *Mater. Chem. Phys.* **2018**, *210*, 126–135. [CrossRef]

Disclaimer/Publisher's Note: The statements, opinions and data contained in all publications are solely those of the individual author(s) and contributor(s) and not of MDPI and/or the editor(s). MDPI and/or the editor(s) disclaim responsibility for any injury to people or property resulting from any ideas, methods, instructions or products referred to in the content.